

Dynamic Models of Spherical Parallel Robots for Model-Based Control Schemes

Ali Hassani^a, Abbas Bataleblu^a, S. A. Khalilpour^a, Hamid D. Taghirad^{a,*}, Philippe Cardou^b

^a*Advanced Robotics and Automated Systems (ARAS), Faculty of Electrical and Computer Engineering, K.N. Toosi University of Technology, Tehran, Iran.*

^b*Department of Mechanical Engineering, Robotics Laboratory, Laval University, Quebec City, QC G1V 0A6, Canada.*

Abstract

In this paper, derivation of different forms of dynamic formulation of spherical parallel robots (SPRs) is investigated. These formulations include the explicit dynamic forms, linear regressor, and Slotine-Li (S-L) regressor, which are required for the design and implementation of the vast majority of model-based controllers and dynamic parameters identification schemes. To this end, the implicit dynamic of SPRs is first formulated using the principle of virtual work in task-space, and then by using an extension, their explicit dynamic formulation is derived. The dynamic equation is then analytically reformulated into linear and S-L regression form with respect to the inertial parameters, and by using the Gauss-Jordan procedure, it is reduced to a unique and closed-form structure. Finally, to illustrate the effectiveness of the proposed method, two different SPRs, namely, the ARAS-Diamond, and the 3-RRR, are examined as the case studies. The obtained results are verified by using the MSC-ADAMS[®] software, and are shared to interested audience for public access.

Keywords: Spherical Parallel Robots, Virtual Work Method, Explicit Dynamic Formulation, Spherical Parallel Robots Dynamics, Model-Based Control

1. Introduction

The demand for precise robotic manipulators is consistently increasing in the industry. Parallel robots (PRs) may suitably address this requirement. Having closed kinematic chains in their structure, PRs often possess higher stiffnesses, accuracies, speeds, and accelerations than their serial counterparts. Spherical parallel robots (SPRs) are a special category of PRs, in which the moving platform and the other moving links, are constrained to rotate about a single point, namely, the center of rotation (CR) [1]¹. Although SPRs are made in various designs and target different applications, perhaps their substantial utilization is to rotate a specific object about a specific point, such as camera attitude [2] or minimally invasive surgeries (MIS) [3].

The dynamic models of robots are needed for model-based controller design, dynamic performance analysis, robot design, and system identification. However, deriving the dynamic model of PRs is a challenging issue, due to inherent complexity, due to their closed-loop structure and kinematic constraints. The issue of the dynamic derivation of PRs is a popular topic in the literature and has been addressed in various papers [4–16] and text-books [17–22]. In general, the dynamic models of PRs may be derived in the joint-

*Corresponding author

Email addresses: hassani@email.kntu.ac.ir (Ali Hassani), a.bataleblu@mail.kntu.ac.ir (Abbas Bataleblu), khalilpour@ee.kntu.ac.ir (S. A. Khalilpour), taghirad@kntu.ac.ir (Hamid D. Taghirad), pcardou@gmc.ulaval.ca (Philippe Cardou)

¹It should be noted that in a group of PRs, the moving-platform and some of the links are constrained to rotate about CR, for example 3-UPU wrist. These robots are outside the scope of this article.

or task-space coordinates. However, it is advantageous to express the actuating joint generalized forces of PRs as a function of the task space variables, since the natural description of PRs dynamics is in the task space, and in addition, the variables to be controlled are naturally defined in the task space [7, 23].

There are several different forms of robot dynamics that are suitable for designing model-based controllers and dynamic calibration procedures. The most common form is the explicit dynamics form, in which robot dynamics is divided into three components: mass terms, Coriolis and centrifugal acceleration terms, and gravity terms. The common inverse dynamic controller (IDC), which is the basis of many advanced model-based controllers, is based on this form. However, there are always structural and parametric uncertainties in the robot dynamic model, which can reduce the performance of IDC [20], and that makes IDC to be the basis for further robust and adaptive controllers for motion tracking control of PRs.

The second derivation form of robot dynamics is the linear regression form. A large class of adaptive control schemes [24, 25], as well as many dynamic calibration procedures [26], requires a regression form that is linear with respect to the parameters of the robot. Thanks to the linear form of the robot dynamics, dynamic model uncertainties may be estimated by adaptive controllers in the feedback loop, or identified using linear regression techniques [27]. Furthermore, there is another type of linear regressor form of the robot dynamics introduced by Slotine and Li in [28]. This regressor form is more suitable for the implementation of adaptive controller structures. In Slotine-Li (S-L) regressor, restrictive requirements are eliminated, such as the need for the acceleration measurement and the computation of the inverse mass matrix.

The main objective of this paper is to derive different forms of dynamics of a general SPR, in order to design different model-based controllers and dynamic identification schemes. By examining the literature on the subject of various controllers designed for SPRs, reported in Table 1, it can be seen that most of reported structures used kinematic-based or simple model-based controllers [1]. Furthermore, it is quite clear that the controllers that use the dynamic information in their control law, may lead to better performance [20, 23].

Table 1: Review of notable control schemes for motion control of SPRs.

Controller	Ref	Method	Robot	Considerations
PID	[29]	Practical	PKAnkle	Poor performance
PID/Kinematic sliding mode	[30]	Practical	2-DOF 5R	— —
PD/PID	[31]	Practical	2-DOF 5R	Only Stabilization
Kinematic sliding mode	[32]	Practical	2-DOF 5R	— —
Kinematic robust adaptive	[33]	Practical	3- <u>R</u> RR	— —
\mathcal{H}_∞	[34]	Practical	ARAS-Diamond	Model Identification
PD+G	[35]	Simulation	Redundant 3-RRR	Uncertainties in the dynamic model
PD+G	[36]	Practical	SHaDe	— —
PD/IDC	[37]	Simulation	3- <u>R</u> RR	— —
IDC	[38]	Simulation	3- <u>R</u> RR	— —
Dynamic robust adaptive switching learning	[39]	Simulation	3- <u>R</u> RR	— —

It seems that a lack of sufficient knowledge about derivation of dynamic model forms of SPRs has limited the use of model-based controllers for SPRs. In order to investigate the different methods for deriving the dynamic models of different SPRs, we re-examined the literature, and report the result in Table 2.

As it is seen in this table in most cases, the derived dynamic models are not complete enough to be used in the design of model-based controllers. Deriving the appropriate dynamic model to identify the robot's dynamic parameters is more critical, where Ref. [52] addresses this issue, but only for the special case of 2DOF-5R SPRs. In addition, the derivation of the S-L regressor, which is necessary for designing various

Table 2: Review of notable dynamic models for different SPRs.

Ref	Approach	Explicit Dynamics	Linear Regressor	S-L Regressor	Case Study
[40]	Newton-Euler	×	×	×	2DOF-5R
[41]	Lagrange	×	×	×	3- <u>RRR</u>
[42, 43]	Virtual Work	×	×	×	2DOF-5R
[44, 45]	— —	×	×	×	3- <u>RRP</u>
[46]	— —	×	×	×	3- <u>RRR</u>
[47]	Gibbs-Appelle	✓	×	×	3- <u>RRR</u>
[48]	Natural Orthogonal Complement	✓	×	×	3- <u>RRP</u>
[38, 39, 49]	Lagrange	✓	×	×	3- <u>RRR</u>
[50, 51]	Virtual Work	✓	×	×	3- <u>RRP</u> , 3- <u>PRR</u>
[52]	Virtual Work	×	✓	×	2DOF-5R
This Paper	Virtual Work	✓	✓	✓	2DOF-5R, and 3- <u>RRR</u>

adaptive controllers, is not reported for any SPR robot in the literature.

In this paper, different forms of the dynamics of SPRs will be examined in detail using the principle of virtual work while the foremost contributions are summarized as follows:

1. Providing a systematic method of deriving explicit dynamic model of a general SPR.
2. Expanding the implicit dynamic formulation to derive linear regressor form, which allows the design a class of adaptive controllers [24, 25].
3. Deriving the reduced regressor matrix using the unique solution, in order to use a wide range of robot dynamic calibration schemes, for example, BIRDy (Benchmark for identification of robot dynamics) MATLAB toolbox [53]. It should be noted that the BIRDy toolbox can only be used for serial manipulators.
4. Using the explicit dynamic formulation and linear regressor form to derive the S-L regressor form of SPRs, in order to be used in many adaptive position/force control schemes, as in [54, 55].

To the best of the authors’ knowledge, such formulation has never been presented in the literature before. Previous formulations usually are case dependent, which cannot be generalized into a systematic method of dynamic formulation. Or they provide only one of these dynamic forms, which is not sufficient to be used for the advanced control structures of the position/force of SPRs. To demonstrate the scope of the dynamic formulation derived in this paper in terms of structure synthesis, different SPRs are referred to, while two different SPRs, namely, ARAS-Diamond (2-DOF 5R), and 3-RRR, are considered as the case studies. The results of the derived dynamics model are made publicly available ².

The remainder of this paper is organized as follows. Implicit and explicit dynamic analysis are presented in section 2, while section 3 describes the linear regressor and the Slotine-Li regressor analysis of SPRs. Then, the dynamic analysis on two case studies is reported in section 4, and the simulation and validation results by using MSC-ADAMS[®] software is given in section 5. Finally, the concluding remarks are given in the last section.

2. Dynamic Analysis

2.1. Preliminary Definitions

In this section, preliminary definitions for the dynamic formulation of SPRs are given. The structure of these robots consists of several links and a moving platform with pure rotational motion about the CR point.

²[Github.com/aras-labs/SPRs_Dynamic_Model](https://github.com/aras-labs/SPRs_Dynamic_Model)

The origin of the base coordinate system is set at the CR point, as shown in the schematic of Figure 1.

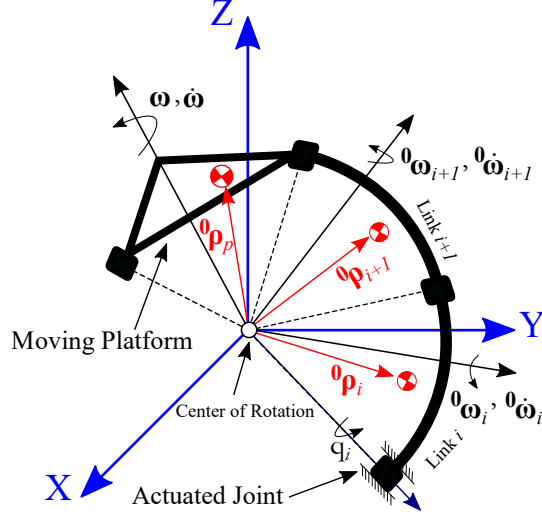


Figure 1: View of a SPR

Throughout this paper, the i and p indices refer to each link and to the moving platform, respectively. Moreover, $\mathbf{q} = [q_1 \dots q_j]^T$ denotes the actuated joint variables, while $\boldsymbol{\chi}$ represents independent generalized parameters of the moving platform. In SPRs, the moving platform has pure rotation about the CR point, and therefore, $\boldsymbol{\chi}$ may be considered as $\boldsymbol{\chi} = \boldsymbol{\theta} = [\theta_1, \theta_2, \theta_3]^T$. In addition, to describe the orientation of the moving platform in the task space coordinate, different approaches are reported in the literature. In this paper, Euler angles and the spherical base coordinate system are adopted. Besides, $S(\mathbf{a})$ denotes the 3×3 skew-symmetric matrix generated from the vector $\mathbf{a} = [a_1, a_2, a_3]^T$.

2.2. The Principle of Virtual Work for Parallel Robots

The principle of virtual work for a PR with several links and a moving platform, may be stated as [9]:

$$\delta W = \delta \mathbf{q}^T \cdot \boldsymbol{\tau} + \delta \boldsymbol{\chi}_p^T \cdot \mathbf{f}_p + \sum_{i=1}^k \left(\delta \boldsymbol{\chi}_i^T \cdot \mathbf{f}_i \right) = 0, \quad (1)$$

where $\delta \boldsymbol{\chi}_p = [\delta \mathbf{x}_p^T, \delta \boldsymbol{\theta}_p^T]^T$ and $\delta \boldsymbol{\chi}_i = [\delta \mathbf{x}_i^T, \delta \boldsymbol{\theta}_i^T]^T$ represent the virtual displacements of the CGs of the moving platform and of link i , respectively. Furthermore, \mathbf{f}_p and \mathbf{f}_i denote the inertial wrenches respectively applied at the moving platform CG and the i th link CG. Moreover, k indicates the number of links. These inertial wrenches take the form:

$$\mathbf{f}_p = \begin{bmatrix} \mathbf{f}_p \\ \mathbf{n}_p \end{bmatrix} = - \begin{bmatrix} m_p ({}^0\mathbf{a}_p - \mathbf{g}_0) - \mathbf{f}_{G_d} \\ ({}^0\mathbf{I}_p {}^0\dot{\boldsymbol{\omega}} + {}^0\boldsymbol{\omega} \times ({}^0\mathbf{I}_p {}^0\boldsymbol{\omega})) - \mathbf{n}_{G_d} \end{bmatrix}, \quad (2a)$$

$$\mathbf{f}_i = \begin{bmatrix} \mathbf{f}_i \\ \mathbf{n}_i \end{bmatrix} = - \begin{bmatrix} m_i ({}^0\mathbf{a}_i - \mathbf{g}_0) \\ ({}^0\mathbf{I}_i {}^0\dot{\boldsymbol{\omega}}_i + {}^0\boldsymbol{\omega}_i \times ({}^0\mathbf{I}_i {}^0\boldsymbol{\omega}_i)) \end{bmatrix}, \quad (2b)$$

in which ${}^0\mathbf{a}_p$ denotes the linear acceleration of CG of the moving platform, and ${}^0\mathbf{I}_p$ denotes the inertia matrix of the moving platform about its CG and expressed in the base coordinate system. Moreover, ${}^0\boldsymbol{\omega}$ and ${}^0\dot{\boldsymbol{\omega}}$ respectively represent the angular velocity and acceleration of the moving platform. Similar to this notation, the same is applied to each link's inertial force with index i . In addition, $\mathbf{f}_{G_d} = [\mathbf{f}_{G_d}^T, \mathbf{n}_{G_d}^T]^T$ is an external disturbance wrench applied on the moving platform CG.

By choosing the $\delta\mathcal{X} = \delta\mathcal{X}_p$ as the independent generalized virtual displacements of the PR, virtual displacement of links, $\delta\mathbf{q}$, may be related to the virtual displacement of the moving platform, $\delta\mathcal{X}$, by the manipulator Jacobian $\mathbf{J} = [\mathbf{J}_v^T, \mathbf{J}_\omega^T]^T$ as:

$$\delta\mathbf{q} = \mathbf{J} \delta\mathcal{X}. \quad (3)$$

Furthermore, the virtual displacement of the CG of link i , $\delta\mathcal{X}_i$, may be related to $\delta\mathcal{X}$ by a Jacobian matrix defined for each link and denoted by $\mathbf{J}_i = [\mathbf{J}_{v_i}^T, \mathbf{J}_{\omega_i}^T]^T$ as:

$$\delta\mathcal{X}_i = \mathbf{J}_i \delta\mathcal{X}. \quad (4)$$

Substituting (3) and (4) into equation of (1) results in:

$$\delta\mathcal{X}^T \left(\mathbf{J}^T \boldsymbol{\tau} + \mathbf{f}_p + \sum_{i=1}^k \mathbf{J}_i^T (\mathbf{f}_i) \right) = 0. \quad (5)$$

Finally, the implicit dynamics formulation of PRs may be represented as follows:

$$\mathbf{f} = \mathbf{J}^T \boldsymbol{\tau} = - \left(\mathbf{f}_p + \sum_{i=1}^k \mathbf{J}_i^T (\mathbf{f}_i) \right). \quad (6)$$

In general, $\mathbf{f} = [\mathbf{f}^T, \mathbf{n}^T]^T = \mathbf{J}^T \boldsymbol{\tau}$ is defined as a mapping of the actuator forces $\boldsymbol{\tau}$ into the space of moving platform wrenches. Therefore, the Jacobian matrix is a squared matrix if the robot is fully parallel with no redundancy in actuators. Accordingly, in non-singular configurations, actuator forces may uniquely be derived as $\boldsymbol{\tau} = \mathbf{J}^{-T} \mathbf{f}$.

As mentioned before, this formulation is based on the kinematic analysis of the CG of each link and of the moving platform. However, if external wrenches (2) are applied to an arbitrary point \mathcal{A} distinct from the CG, the external wrenches equation may be rewritten according to this arbitrary point. It may be proved that the principle of virtual work for any arbitrary point \mathcal{A} in PRs is derived as [56]:

$$\delta W = \delta\mathbf{q}^T \cdot \boldsymbol{\tau} + \delta\mathcal{X}_{\mathcal{A}_p}^T \cdot \mathbf{f}_{\mathcal{A}_p} + \sum_{i=1}^k \left(\delta\mathcal{X}_{\mathcal{A}_i}^T \cdot \mathbf{f}_{\mathcal{A}_i} \right) = 0, \quad (7)$$

in which, $\delta\mathcal{X}_{\mathcal{A}_p} = [\delta\mathbf{x}_{\mathcal{A}_p}^T, \delta\boldsymbol{\theta}_{\mathcal{A}_p}^T]^T$ and $\delta\mathcal{X}_{\mathcal{A}_i} = [\delta\mathbf{x}_{\mathcal{A}_i}^T, \delta\boldsymbol{\theta}_{\mathcal{A}_i}^T]^T$ indicate virtual displacements of any arbitrary point \mathcal{A} of the moving platform and each link, respectively. Therefore, inertial forces of the moving platform and each link with respect to this arbitrary point may be derived as:

$$\mathbf{f}_{\mathcal{A}_p} = \begin{bmatrix} \mathbf{f}_{\mathcal{A}_p} \\ \mathbf{n}_{\mathcal{A}_p} \end{bmatrix} = - \begin{bmatrix} m_p ({}^0\dot{\boldsymbol{\omega}} \times {}^0\rho_p + {}^0\boldsymbol{\omega} \times ({}^0\boldsymbol{\omega} \times {}^0\rho_p) + ({}^0\mathbf{a}_{\mathcal{A}_p} - \mathbf{g}_0)) - \mathbf{f}_d \\ ({}^0\mathbf{I}_{\mathcal{A}_p} {}^0\dot{\boldsymbol{\omega}} + {}^0\boldsymbol{\omega} \times ({}^0\mathbf{I}_{\mathcal{A}_p} {}^0\boldsymbol{\omega}) + m_p {}^0\rho_p \times ({}^0\mathbf{a}_{\mathcal{A}_p} - \mathbf{g}_0)) - \mathbf{n}_d \end{bmatrix}, \quad (8a)$$

$$\mathbf{f}_{\mathcal{A}_i} = \begin{bmatrix} \mathbf{f}_{\mathcal{A}_i} \\ \mathbf{n}_{\mathcal{A}_i} \end{bmatrix} = - \begin{bmatrix} m_i ({}^0\dot{\boldsymbol{\omega}}_i \times {}^0\rho_i + {}^0\boldsymbol{\omega}_i \times ({}^0\boldsymbol{\omega}_i \times {}^0\rho_i) + ({}^0\mathbf{a}_{\mathcal{A}_i} - \mathbf{g}_0)) \\ ({}^0\mathbf{I}_{\mathcal{A}_i} {}^0\dot{\boldsymbol{\omega}}_i + {}^0\boldsymbol{\omega}_i \times ({}^0\mathbf{I}_{\mathcal{A}_i} {}^0\boldsymbol{\omega}_i) + m_i {}^0\rho_i \times ({}^0\mathbf{a}_{\mathcal{A}_i} - \mathbf{g}_0)) \end{bmatrix}, \quad (8b)$$

in which, ${}^0\mathbf{a}_{\mathcal{A}_p}$ denotes the acceleration of point \mathcal{A}_p in the base coordinate system. The vector ${}^0\rho_p$, points from the arbitrary point \mathcal{A}_p to the origin of the base coordinate system. It must be noted that equal notation applies to the inertial forces of each link with the index of i . Moreover, we define $\mathbf{f}_d = [\mathbf{f}_d^T, \mathbf{n}_d^T]^T$ as the external disturbance wrench applied on the moving platform at the arbitrary point \mathcal{A}_p .

Therefore, PRs' dynamic formulation may be derived analogously to the process mentioned in equations of (3) and (4). The only difference, however, is the kinematic analysis, which is based on the arbitrary points \mathcal{A}_i and \mathcal{A}_p , for each link and the moving platform, respectively. Thus, in the following, this general formulation is used to derive a simple form of the SPR dynamics.

2.3. Implicit Dynamic Analysis of Spherical Parallel Robots

As mentioned earlier, in SPRs, the moving platform undergoes pure rotations about the CR point. Accordingly, we propose expressing the dynamic formulations in a coordinate system with its origin at the CR. Hence, by selecting $\mathcal{A}_i = \mathcal{A}_p$ as a fixed point at the origin of the base coordinate system, all links and the moving platform experience pure rotations about the CR point. As a result, the virtual linear displacement of points of \mathcal{A}_i and \mathcal{A}_p always remains zero. This implies that, the substitution of $\delta\theta_{\mathcal{A}_p}$ and $\delta\theta_{\mathcal{A}_i}$ into Eq. (7) leads to $\delta\mathbf{q} = \mathbf{J}_\omega \delta\theta$ and $\delta\theta_i = \mathbf{J}_{\omega_i} \delta\theta$. Therefore, the dynamic formulation of SPRs may be accomplished as follows, which would be interpreted as the implicit dynamic formulation of SPRs:

$$\mathbf{J}_\omega^T \boldsymbol{\tau} = \mathbf{n} + \mathbf{n}_d = \mathbf{n}_p + \sum_{i=1}^k \mathbf{n}_i, \quad \in \mathbb{R}^m, \quad (9)$$

in which, $\mathbf{J}_\omega^T \boldsymbol{\tau} = \mathbf{n} + \mathbf{n}_d$ represents the mapping of the actuator forces $\boldsymbol{\tau}$ on moving platform moments. Moreover, m denotes the number of generalized task space variables, and the \mathbf{n}_p and \mathbf{n}_i are defined as:

$$\mathbf{n}_p = {}^0\mathbf{I}_{\mathcal{A}_p} {}^0\dot{\boldsymbol{\omega}} + S({}^0\boldsymbol{\omega}) ({}^0\mathbf{I}_{\mathcal{A}_p} {}^0\boldsymbol{\omega}) - m_p S({}^0\rho_p) \mathbf{g}_0, \quad (10a)$$

$$\mathbf{n}_i = \mathbf{J}_{\omega_i}^T ({}^0\mathbf{I}_{\mathcal{A}_i} {}^0\dot{\boldsymbol{\omega}}_i + S({}^0\boldsymbol{\omega}_i) ({}^0\mathbf{I}_{\mathcal{A}_i} {}^0\boldsymbol{\omega}_i) - m_i S({}^0\rho_i) \mathbf{g}_0), \quad (10b)$$

where, $S(\mathbf{a})$ represents the 3×3 skew-symmetric matrix of vector \mathbf{a} and the following mapping may be used for deriving $S({}^0\rho_i)$ and, likewise, $S({}^0\rho_p)$:

$$S({}^0\rho_i) = {}^0\mathbf{R}_i S({}^i\rho_i) {}^0\mathbf{R}_i^T. \quad (11)$$

in which, ${}^0\mathbf{R}_i$ denotes the rotation matrix of each link, respect to base coordinate system, and ${}^i\rho_i$ is the center of gravity (CG) position of link i respect to its CG.

2.4. Explicit Dynamic Analysis of Spherical Parallel Robots

As stated before, the orientation of the moving platform of SPRs might be determined by their generalized coordinate, while its derivatives represent the angular velocity and the angular acceleration as $\dot{\boldsymbol{\theta}} = {}^0\boldsymbol{\omega}$, and $\ddot{\boldsymbol{\theta}} = {}^0\dot{\boldsymbol{\omega}}$. In addition, the angular velocity and acceleration of each link may be expressed as:

$${}^0\boldsymbol{\omega}_i = \mathbf{J}_{\omega_i} \dot{\boldsymbol{\theta}}, \quad (12a)$$

$${}^0\dot{\boldsymbol{\omega}}_i = \mathbf{J}_{\omega_i} \ddot{\boldsymbol{\theta}} + \dot{\mathbf{J}}_{\omega_i} \dot{\boldsymbol{\theta}}. \quad (12b)$$

In order to derive the explicit form of the dynamic formulations employing the principle of virtual work, substitute (12) into the implicit dynamic formulation of (9). With some manipulations, the explicit dynamic formulation for SPRs is written as:

$$\mathbf{J}_\omega^T \boldsymbol{\tau} = \mathbf{n} + \mathbf{n}_d = \mathbf{M}(\boldsymbol{\theta}) \ddot{\boldsymbol{\theta}} + \mathbf{C}(\boldsymbol{\theta}, \dot{\boldsymbol{\theta}}) \dot{\boldsymbol{\theta}} + \mathbf{g}(\boldsymbol{\theta}), \quad (13)$$

in which,

$$\mathbf{M}(\boldsymbol{\theta}) = {}^0\mathbf{I}_{\mathcal{A}_p} + \sum_{i=1}^k \left(\mathbf{J}_{\omega_i}^T {}^0\mathbf{I}_{\mathcal{A}_i} \mathbf{J}_{\omega_i} \right), \quad (14a)$$

$$\mathbf{C}(\boldsymbol{\theta}, \dot{\boldsymbol{\theta}}) = S(\boldsymbol{\omega}) {}^0\mathbf{I}_{\mathcal{A}_p} + \sum_{i=1}^k \mathbf{J}_{\omega_i}^T \left({}^0\mathbf{I}_{\mathcal{A}_i} \dot{\mathbf{J}}_{\omega_i} + S(\mathbf{J}_{\omega_i} \dot{\boldsymbol{\theta}}) {}^0\mathbf{I}_{\mathcal{A}_i} \mathbf{J}_{\omega_i} \right), \quad (14b)$$

$$\mathbf{g}(\boldsymbol{\theta}) = -m_p S({}^0\rho_p) \mathbf{g}_0 - m_i \sum_{i=1}^k \mathbf{J}_{\omega_i}^T S({}^0\rho_i) \mathbf{g}_0. \quad (14c)$$

In order to use the CG position of each link in the body coordinate system instead of the base coordinate system, we substitute (11) into (14c), which yields:

$$\mathbf{g}(\boldsymbol{\theta}) = -m_i \left({}^0\mathbf{R}_p S({}^p\rho_p) {}^0\mathbf{R}_p^T \right) \mathbf{g}_0 - m_i \sum_{i=1}^k \mathbf{J}_{\omega_i}^T \left({}^0\mathbf{R}_i S({}^i\rho_i) {}^0\mathbf{R}_i^T \right) \mathbf{g}_0. \quad (15)$$

The dynamic matrices of the explicit dynamic formulation of SPRs obtained in equation (13) satisfy two important properties, which might be used in the design of model-based controllers [54]:

Property 1. Matrix $\mathbf{M}(\boldsymbol{\theta})$ is positive definite in all configurations.

Property 2. The matrix $\left[\dot{\mathbf{M}}(\boldsymbol{\theta}, \dot{\boldsymbol{\theta}}) - 2\mathbf{C}(\boldsymbol{\theta}, \dot{\boldsymbol{\theta}}) \right]$ is skew-symmetric.

The first property may be easily proved, considering the quadratic structure of its expression in Eq. (14a). Proving the second property is less straight forward. First, the time derivative of $\mathbf{M}(\boldsymbol{\theta})$ may be computed as:

$$\begin{aligned} \dot{\mathbf{M}} &= \left(S({}^0\boldsymbol{\omega}) {}^0\mathbf{I}_{A_p} + {}^0\mathbf{I}_{A_p} S({}^0\boldsymbol{\omega})^T \right) + \sum_{i=1}^k \dot{\mathbf{J}}_{\omega_i}^T {}^0\mathbf{I}_{A_i} \mathbf{J}_{\omega_i} \\ &\quad + \mathbf{J}_{\omega_i}^T \left(S({}^0\boldsymbol{\omega}_i) {}^0\mathbf{I}_{A_i} + {}^0\mathbf{I}_{A_i} S({}^0\boldsymbol{\omega}_i)^T \right) \mathbf{J}_{\omega_i} + \mathbf{J}_{\omega_i}^T {}^0\mathbf{I}_{A_i} \dot{\mathbf{J}}_{\omega_i}. \end{aligned} \quad (16)$$

Therefore, it can be easily verified that:

$$\left(\dot{\mathbf{M}}(\boldsymbol{\theta}, \dot{\boldsymbol{\theta}}) - 2\mathbf{C}(\boldsymbol{\theta}, \dot{\boldsymbol{\theta}}) \right)^T + \left(\dot{\mathbf{M}}(\boldsymbol{\theta}, \dot{\boldsymbol{\theta}}) - 2\mathbf{C}(\boldsymbol{\theta}, \dot{\boldsymbol{\theta}}) \right) = 0. \quad (17)$$

3. Regressor Analysis

3.1. Slotine-Li Regressor

In the S-L adaptive controller, the control effort in the task-space is defined as [28]:

$$\mathbf{M}(\boldsymbol{\theta})\ddot{\boldsymbol{\theta}}_r + \mathbf{C}(\boldsymbol{\theta}, \dot{\boldsymbol{\theta}})\dot{\boldsymbol{\theta}}_r + \mathbf{g}(\boldsymbol{\theta}) - \mathbf{K}\mathbf{s} = \mathbf{Y}_S(\boldsymbol{\theta}, \dot{\boldsymbol{\theta}}, \ddot{\boldsymbol{\theta}}_r, \ddot{\boldsymbol{\theta}}_r)\boldsymbol{\pi} - \mathbf{K}\mathbf{s}, \quad (18)$$

in which, the error is defined as $\mathbf{e} = \boldsymbol{\theta} - \boldsymbol{\theta}_d$, whereas $\boldsymbol{\theta}_d$ denotes the desired trajectory in the task-space. Moreover, the reference velocity of $\dot{\boldsymbol{\theta}}_r$ is defined as $\dot{\boldsymbol{\theta}}_r = \dot{\boldsymbol{\theta}}_d - \boldsymbol{\Lambda}\mathbf{e}$, and $\mathbf{s} = \dot{\boldsymbol{\theta}} - \dot{\boldsymbol{\theta}}_r = \dot{\mathbf{e}} + \boldsymbol{\Lambda}\mathbf{e}$ indicates the sliding surface. Furthermore, \mathbf{K} and $\boldsymbol{\Lambda}$ represent symmetric positive definite gains while, $\mathbf{Y}_S(\boldsymbol{\theta}, \dot{\boldsymbol{\theta}}, \ddot{\boldsymbol{\theta}}_r, \ddot{\boldsymbol{\theta}}_r)$ is known as the Slotine-Li regressor.

In order to derive this regressor for SPRs, $\mathbf{M}(\boldsymbol{\theta})$, $\mathbf{C}(\boldsymbol{\theta}, \dot{\boldsymbol{\theta}})$, and $\mathbf{g}(\boldsymbol{\theta})$ are substituted into Eq. (18). By this means, the following relation is derived:

$$\mathbf{n}_S + \mathbf{n}_d = \mathbf{n}_{S_p} + \sum_{i=1}^k \mathbf{n}_{S_i}, \quad (19a)$$

$$\mathbf{n}_{S_p} = ({}^0\mathbf{I}_{A_p}) \ddot{\boldsymbol{\theta}}_r + (S({}^0\boldsymbol{\omega}) {}^0\mathbf{I}_{A_p}) \dot{\boldsymbol{\theta}}_r - m_p S({}^0\rho_p) \mathbf{g}_0, \quad (19b)$$

$$\begin{aligned} \mathbf{n}_{S_i} &= \mathbf{J}_{\omega_i}^T \left(({}^0\mathbf{I}_{A_i} \mathbf{J}_{\omega_i}) \ddot{\boldsymbol{\theta}}_r + ({}^0\mathbf{I}_{A_i} \dot{\mathbf{J}}_{\omega_i} + S(\mathbf{J}_{\omega_i} \dot{\boldsymbol{\theta}}) {}^0\mathbf{I}_{A_i} \mathbf{J}_{\omega_i}) \dot{\boldsymbol{\theta}}_r + \dots \right. \\ &\quad \left. - m_i S({}^0\rho_i) \mathbf{g}_0 \right). \end{aligned} \quad (19c)$$

Analogous to Eq. (12), it is clear that ${}^0\boldsymbol{\omega}_{r_i} = \mathbf{J}_{\omega_i} \dot{\boldsymbol{\theta}}_r$ and ${}^0\dot{\boldsymbol{\omega}}_{r_i} = \mathbf{J}_{\omega_i} \ddot{\boldsymbol{\theta}}_r + \dot{\mathbf{J}}_{\omega_i} \dot{\boldsymbol{\theta}}_r$. Furthermore, for SPRs, it may be considered that $\dot{\boldsymbol{\theta}}_r = {}^0\boldsymbol{\omega}_r$ and $\ddot{\boldsymbol{\theta}}_r = {}^0\dot{\boldsymbol{\omega}}_r$. Hence, the following relation is derived by substituting these formulas into Eq. (21):

$$\mathbf{n}_{S_i} = \mathbf{J}_{\omega_i}^T \left({}^0\mathbf{I}_{A_i} {}^0\dot{\boldsymbol{\omega}}_{r_i} + S({}^0\boldsymbol{\omega}_i) ({}^0\mathbf{I}_{A_i} {}^0\boldsymbol{\omega}_{r_i}) - m_i S({}^0\rho_i) \mathbf{g}_0 \right), \quad (20a)$$

$$\mathbf{n}_{S_p} = ({}^0\mathbf{I}_{A_p}) {}^0\dot{\boldsymbol{\omega}}_r + (S({}^0\boldsymbol{\omega}) {}^0\mathbf{I}_{A_p}) {}^0\boldsymbol{\omega}_r - m_p S({}^0\rho_p) \mathbf{g}_0. \quad (20b)$$

To derive the S-L regressor from equation (20), one may use ${}^0\dot{\boldsymbol{\omega}}_{r_i} = {}^0\mathbf{R}_i {}^i\dot{\boldsymbol{\omega}}_{r_i}$, ${}^0\boldsymbol{\omega}_{r_i} = {}^0\mathbf{R}_i {}^i\boldsymbol{\omega}_{r_i}$, ${}^0\mathbf{I}_{\mathcal{A}_i} = {}^0\mathbf{R}_i {}^i\mathbf{I}_{\mathcal{A}_i} {}^0\mathbf{R}_i^T$, and Eq. (11). Therefore, different parts of equation of (20a) will be rewritten as follows:

$${}^0\mathbf{I}_{\mathcal{A}_i} {}^0\dot{\boldsymbol{\omega}}_{r_i} = {}^0\mathbf{R}_i ({}^i\mathbf{I}_{\mathcal{A}_i} {}^i\dot{\boldsymbol{\omega}}_{r_i}), \quad (21a)$$

$$S({}^0\boldsymbol{\omega}_i) ({}^0\mathbf{I}_{\mathcal{A}_i} {}^0\boldsymbol{\omega}_{r_i}) = {}^0\mathbf{R}_i (S({}^i\boldsymbol{\omega}_i) ({}^i\mathbf{I}_{\mathcal{A}_i} {}^i\boldsymbol{\omega}_{r_i})), \quad (21b)$$

$$-m_i S({}^0\boldsymbol{\rho}_i) \mathbf{g}_0 = -m_i {}^0\mathbf{R}_i S({}^i\boldsymbol{\rho}_i) {}^0\mathbf{R}_i^T \mathbf{g}_0. \quad (21c)$$

Considering ${}^i\mathbf{g}_0 = {}^0\mathbf{R}_i^T \mathbf{g}_0$, and using $S({}^i\boldsymbol{\rho}_i) {}^i\mathbf{g}_0 = -S({}^i\mathbf{g}_0) {}^i\boldsymbol{\rho}_i$, Eq. (21c) will be rewritten as:

$$-m_i S({}^0\boldsymbol{\rho}_i) \mathbf{g}_0 = {}^0\mathbf{R}_i S({}^i\mathbf{g}_0) (m_i {}^i\boldsymbol{\rho}_i). \quad (22)$$

A similar process may be applied to the derivation of the S-L regression form of the moving platform dynamic formulation. Notice that ${}^p\dot{\boldsymbol{\omega}}_r = {}^0\mathbf{R}_p^T {}^0\dot{\boldsymbol{\omega}}_r$, ${}^p\boldsymbol{\omega}_r = {}^0\mathbf{R}_p^T {}^0\boldsymbol{\omega}_r$, ${}^0\mathbf{I}_{\mathcal{A}_p} = {}^0\mathbf{R}_p {}^i\mathbf{I}_{\mathcal{A}_p} {}^0\mathbf{R}_p^T$, and ${}^p\mathbf{g}_0 = {}^0\mathbf{R}_p^T \mathbf{g}_0$. Therefore, the dynamic formulation of the SPRs with respect to the robot's inertial parameters may be rewritten as:

$$\mathbf{n}_{S_i} = \mathbf{J}_{\omega_i}^T {}^0\mathbf{R}_i ({}^i\mathbf{I}_{\mathcal{A}_i} {}^i\dot{\boldsymbol{\omega}}_{r_i} + S({}^i\boldsymbol{\omega}_i) ({}^i\mathbf{I}_{\mathcal{A}_i} {}^i\boldsymbol{\omega}_{r_i}) + S({}^i\mathbf{g}_0) (m_i {}^i\boldsymbol{\rho}_i)), \quad (23a)$$

$$\mathbf{n}_{S_p} = {}^0\mathbf{R}_p ({}^p\mathbf{I}_{\mathcal{A}_p} {}^p\dot{\boldsymbol{\omega}}_r) + S({}^0\boldsymbol{\omega}) {}^0\mathbf{R}_p ({}^p\mathbf{I}_{\mathcal{A}_p} {}^p\boldsymbol{\omega}_r) + S({}^p\mathbf{g}_0) (m_p {}^p\boldsymbol{\rho}_p). \quad (23b)$$

On the other hand, in order to transform the first and second terms of equations of (23a) and (23b) to linear forms, it may be proved that [52, 56]:

$${}^i\mathbf{I}_{\mathcal{A}_i} {}^i\dot{\boldsymbol{\omega}}_{r_i} = {}^i\tilde{\boldsymbol{\omega}}_{r_i} {}^i\bar{\mathbf{I}}_{\mathcal{A}_i}, \quad (24a)$$

$${}^i\mathbf{I}_{\mathcal{A}_i} {}^i\boldsymbol{\omega}_{r_i} = {}^i\tilde{\boldsymbol{\omega}}_{r_i} {}^i\bar{\mathbf{I}}_{\mathcal{A}_i}, \quad (24b)$$

in which, ${}^i\bar{\mathbf{I}}_{\mathcal{A}_i}$ and ${}^i\tilde{\boldsymbol{\omega}}_{r_i}$ are defined as:

$${}^i\bar{\mathbf{I}}_{\mathcal{A}_i} = [I_{xx\mathcal{A}_i}, I_{xy\mathcal{A}_i}, I_{xz\mathcal{A}_i}, I_{yy\mathcal{A}_i}, I_{yz\mathcal{A}_i}, I_{zz\mathcal{A}_i}], \quad (25a)$$

$${}^i\tilde{\boldsymbol{\omega}}_{r_i} = \begin{bmatrix} \omega_{rx_i} & \omega_{ry_i} & \omega_{rz_i} & 0 & 0 & 0 \\ 0 & \omega_{rx_i} & 0 & \omega_{ry_i} & \omega_{rz_i} & 0 \\ 0 & 0 & \omega_{rx_i} & 0 & \omega_{ry_i} & \omega_{rz_i} \end{bmatrix}, \quad (25b)$$

Now, substitute (24) into (23). The linear S-L regressor form of SPRs with respect to the inertial parameters may be derived as:

$$\mathbf{J}_{\omega}^T \boldsymbol{\tau} = \mathbf{n}_S + \mathbf{n}_d = \mathbf{Y}_S(\boldsymbol{\theta}, \dot{\boldsymbol{\theta}}, \ddot{\boldsymbol{\theta}}_r, \ddot{\boldsymbol{\theta}}_r) \boldsymbol{\pi}, \quad (26)$$

in which, the S-L regressor \mathbf{Y}_S is defined as follows:

$$\mathbf{Y}_S = [\mathbf{Y}_{S_p}, \mathbf{Y}_{S_i}, \dots, \mathbf{Y}_{S_n}], \quad (27a)$$

$$\mathbf{Y}_{S_p} = \left[{}^0\mathbf{R}_p S({}^p\mathbf{g}_0), \left({}^0\mathbf{R}_p {}^p\tilde{\boldsymbol{\omega}}_r + S({}^0\boldsymbol{\omega}) {}^0\mathbf{R}_p {}^p\tilde{\boldsymbol{\omega}}_r \right) \right], \quad (27b)$$

$$\mathbf{Y}_{S_i} = \mathbf{J}_{\omega_i}^T {}^0\mathbf{R}_i \left[S({}^i\mathbf{g}_0), \left({}^i\tilde{\boldsymbol{\omega}}_{r_i} + S({}^i\boldsymbol{\omega}_i) {}^i\tilde{\boldsymbol{\omega}}_{r_i} \right) \right]. \quad (27c)$$

and the inertial parameters $\boldsymbol{\pi}$ are defined as:

$$\boldsymbol{\pi} = [\boldsymbol{\pi}_p \quad \boldsymbol{\pi}_i \quad \dots \quad \boldsymbol{\pi}_n]^T, \quad \in \mathbb{R}^{9k}, \quad (28a)$$

$$\boldsymbol{\pi}_p = [m_p {}^p\boldsymbol{\rho}_p \quad {}^p\bar{\mathbf{I}}_{\mathcal{A}_p}]^T, \quad (28b)$$

$$\boldsymbol{\pi}_i = [m_i {}^i\boldsymbol{\rho}_i \quad {}^i\bar{\mathbf{I}}_{\mathcal{A}_i}]^T. \quad (28c)$$

A careful examination of Eq. (28), confirms that, in SPRs, the first moment and the moment of inertia are the only inertial parameters in vector $\boldsymbol{\pi}$, so that the pure masses of the links do not directly contribute to the dynamics. Moreover, in order to derive linear regressor form, it is enough to substitute $\ddot{\boldsymbol{\theta}}_r = \ddot{\boldsymbol{\theta}}$ and $\ddot{\boldsymbol{\theta}}_r = \ddot{\boldsymbol{\theta}}$ in Eq. (27), which leads to ${}^p\tilde{\boldsymbol{\omega}}_r = {}^p\tilde{\boldsymbol{\omega}}$ and ${}^p\tilde{\boldsymbol{\omega}}_r = {}^p\tilde{\boldsymbol{\omega}}$, as well as ${}^i\tilde{\boldsymbol{\omega}}_{r_i} = {}^i\tilde{\boldsymbol{\omega}}_i$ and ${}^i\tilde{\boldsymbol{\omega}}_{r_i} = {}^i\tilde{\boldsymbol{\omega}}_i$.

3.2. Unique Regressor Reduction

Careful examinations of regressor forms stated in Eq. (27) reveal the stringent requirement of order reduction to eliminate the zero or linearly dependent elements in the regressor. In practice, although using a reduced regressor in adaptive model-based controllers does not improve the performance of the controller, it significantly decreases the required real-time computational process. On the other hand, in the calibration schemes in which linear regression form of robot dynamics is used, it is inevitable to use a reduced regressor to avoid having a rank-deficient observation matrix and to make elements of the inertial parameters fully identifiable.

For this means, we want to eliminate the zero or linearly dependent elements in the obtained regressor. For this purpose, the method mentioned in Ref. [57], which has a unique solution, is used. To this end, one may represent the observation matrix of SPRs as:

$$\mathbf{W}(\boldsymbol{\theta}, \dot{\boldsymbol{\theta}}, \ddot{\boldsymbol{\theta}}) = [\mathbf{Y}(t_1)^T \quad \dots \quad \mathbf{Y}(t_k)^T]^T, \quad \in \mathbb{R}^{jm \times 9k}, \quad (29)$$

in which j represents the number of observations. If j is sufficiently large, the condition $jm \geq 9k$ shall be met for the system to be observable. Hence, the reduced regressor matrix \mathbf{Y}_r and the BIPs $\boldsymbol{\pi}_r$ shall be found such that to preserve the full rank p of the observation matrix \mathbf{W} , in order for the system to be observable. In such a case, it may be proved that there is a unique transformation matrix $\mathbf{B} \in \mathbb{R}^{p \times 9k}$ and a matrix \mathbf{S} , spanning the row space of the observation matrix such that there exist a generalized inverse $\mathbf{B}^\dagger = \mathbf{S}\mathbf{B}^T (\mathbf{B}\mathbf{S}\mathbf{B}^T)^{-1}$. In order to derive the \mathbf{B} matrix, it suffices to calculate the reduced-row echelon form of \mathbf{W} , which is the upper triangular matrix \mathbf{B}_E . By eliminating the zero rows of \mathbf{B}_E , the matrix \mathbf{B} is derived. By this means, $\mathbf{Y}_r \in \mathbb{R}^{m \times p}$ and $\boldsymbol{\pi}_r \in \mathbb{R}^p$ are derived as:

$$\mathbf{Y}_r = \mathbf{Y}\mathbf{B}^\dagger, \quad (30a)$$

$$\boldsymbol{\pi}_r = \mathbf{B}\boldsymbol{\pi}. \quad (30b)$$

It should be noted that, the \mathbf{B}_E matrix is only a function of the kinematic parameters of the robot, and has numerical values. Thus, to calculate it, *rref* command in MATLAB can be used for the above mentioned calculations.

4. Examples

To verify the validity of the formulation presented in this paper on different SRRs, the literature was re-examined to select suitable case studies. According to different kinematic architectures, some of the notable SPRs may be listed as:

- **2-DOF SPRs:** SPRs with 5R structures, their various configurations have been widely mentioned in the literature [31, 52]. In addition, SPRs with as 7-bars [58], with 8-bars [59], RR-RRR-RRR [60], and 2-RRR [61] may be listed.
- **3-DOF SPRs:** SPRs with 3-RRR structures [39, 62], 3-RRP [50], 3-RRS [63], and 3-PRR [51].

In this paper, two distinguished SPRs, namely, the ARAS-Diamond (2-DOF 5R) [64], and the standard 3-RRR, are selected as the case studies in this paper. The reasons for choosing these robots are as following:

1. Evaluation of SPRs with different kinematic structures, one example with a 5R structure and the other with a 3-RRR structure. Kinematic analysis of these robots will show how Jacobian matrices and their derivatives (in fact, the terms of angular velocity and acceleration) for each link can be derived.
2. Investigation of different approaches to the description of the orientation of the moving platform in the task space. It will be shown that the use of Euler angles requires minor modifications to the proposed dynamic formulation.

In the next section, the kinematic analysis of the two case studies is examined.

4.1. ARAS-Diamond Robot

The ARAS-Diamond robot is a PR developed to perform the minimally invasive vitreoretinal eye surgery. According to the robot's spherical structure, all the links have a pure rotational motion about the remote center of motion (RCM). The kinematic details of this robot are given in details in [64], and in this article, only its important issues are reviewed.

4.1.1. Robot Geometry

The kinematic structure of the ARAS-Diamond SPR is depicted in Fig. 2. Similar to [64], the position of this point in the spherical coordinate system is considered as the generalized coordinate. Task space variables $\boldsymbol{\theta} = [\phi, \gamma]^T$ are sufficient to describe the position of this point, since the ARAS-Diamond robot structure is designed such that all the links are enclosed in a sphere. As a result, adopting spherical coordinates instead of Cartesian coordinates leads to a simpler kinematic analysis [64].

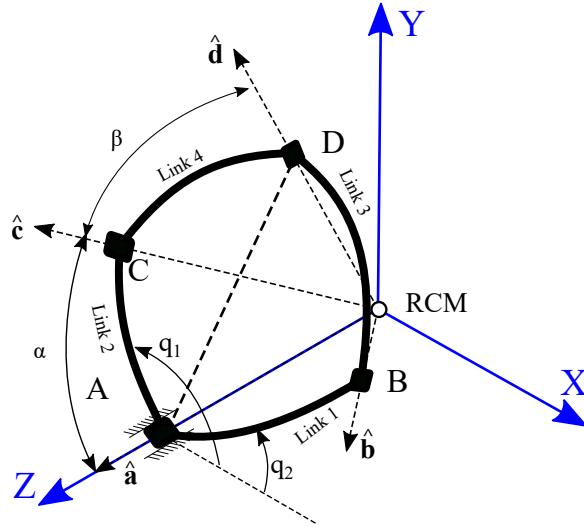


Figure 2: Schematic of the ARAS-Diamond SPR

As illustrated in Fig. 2, the geometric parameters of the robot may be specified by α and β , and the four unit-vectors of $\hat{\mathbf{a}}$, $\hat{\mathbf{b}}$, $\hat{\mathbf{c}}$, and $\hat{\mathbf{d}}$ represent the directions from the RCM point to the revolute joints of the robot as:

$$\hat{\mathbf{a}} = [0, 0, 1]^T, \quad \hat{\mathbf{b}} = \mathbf{R}_z\left(q_2 + \frac{\pi}{2}\right) \mathbf{R}_x(\alpha) \hat{\mathbf{a}}, \quad (31a)$$

$$\hat{\mathbf{c}} = \mathbf{R}_z\left(q_1 + \frac{\pi}{2}\right) \mathbf{R}_x(\alpha) \hat{\mathbf{a}}, \quad \hat{\mathbf{d}} = \mathbf{R}_z(\phi) \mathbf{R}_y(\gamma) \hat{\mathbf{a}}. \quad (31b)$$

4.1.2. Differential Kinematic Analysis

The inverse kinematics of the ARAS-Diamond robot may be expressed as follows [64]:

$$q_1 = \phi + \arccos\left(\frac{\cos \beta - \cos \gamma \cdot \cos \alpha}{\sin \gamma \cdot \sin \alpha}\right), \quad (32a)$$

$$q_2 = \phi - \arccos\left(\frac{\cos \beta - \cos \gamma \cdot \cos \alpha}{\sin \gamma \cdot \sin \alpha}\right). \quad (32b)$$

In order to derive the Jacobian matrix, the time derivative of (32) is computed. Accordingly, \dot{q}_1 and \dot{q}_2 may be represented as:

$$\dot{q}_1 = \dot{\phi} + h \dot{\gamma}, \quad (33a)$$

$$\dot{q}_2 = \dot{\phi} - h \dot{\gamma}, \quad (33b)$$

where, scalar parameter h is given in Appendix Appendix A. Consequently, by arranging (33) into a matrix form, the Jacobian matrix is given as:

$$\mathbf{J}_\omega = \begin{bmatrix} 1 & +h \\ 1 & -h \end{bmatrix}. \quad (34)$$

In order to derive passive joint Jacobians, which map the velocity from the task-space to the passive joints $\dot{\mathbf{q}}_p = [\dot{\hat{C}}, \dot{\hat{B}}]^T$, we must compute $\dot{\hat{C}}$ and $\dot{\hat{B}}$. It can be proved that:

$$\dot{\hat{B}} = -\dot{\hat{C}} = s \dot{\gamma}, \quad (35)$$

in which, the scalar parameter s is given in Appendix Appendix A. As a result, the Jacobian matrix of the passive angles, is obtained as:

$$\mathbf{J}_{\omega_p} = \begin{bmatrix} 0 & -s \\ 0 & +s \end{bmatrix}. \quad (36)$$

4.1.3. Jacobian Analysis of Each Link

In order to calculate the angular velocity of each link of the robot, it is split into two identical serial arms. Hence, the angular velocity of each link may be derived as follows:

$${}^0\boldsymbol{\omega}_1 = \dot{q}_2 \cdot \hat{\mathbf{a}}, \quad (37a)$$

$${}^0\boldsymbol{\omega}_2 = \dot{q}_1 \cdot \hat{\mathbf{a}}, \quad (37b)$$

$${}^0\boldsymbol{\omega}_3 = \dot{q}_2 \cdot \hat{\mathbf{a}} - \dot{\hat{B}} \cdot \hat{\mathbf{b}} = {}^0\boldsymbol{\omega}_1 - \dot{\hat{B}} \cdot \hat{\mathbf{b}}, \quad (37c)$$

$${}^0\boldsymbol{\omega}_4 = \dot{q}_1 \cdot \hat{\mathbf{a}} + \dot{\hat{C}} \cdot \hat{\mathbf{c}} = {}^0\boldsymbol{\omega}_2 + \dot{\hat{C}} \cdot \hat{\mathbf{c}}. \quad (37d)$$

Therefore, the Jacobian matrix of each link is given by:

$$\mathbf{J}_{\omega_1} = [\hat{\mathbf{a}} \quad -h\hat{\mathbf{a}}], \quad \mathbf{J}_{\omega_2} = [\hat{\mathbf{a}} \quad +h\hat{\mathbf{a}}], \quad (38)$$

$$\mathbf{J}_{\omega_3} = \mathbf{J}_{\omega_1} + [\mathbf{0}_{3 \times 1} \quad -s\hat{\mathbf{b}}], \quad \mathbf{J}_{\omega_4} = \mathbf{J}_{\omega_2} + [\mathbf{0}_{3 \times 1} \quad -s\hat{\mathbf{c}}], \quad (39)$$

in which, $\mathbf{0}_{3 \times 1}$ denotes the 3×1 zero vector.

4.1.4. Acceleration Analysis

The derivative of the Jacobian matrix of the first and second links are easily be obtained as:

$$\dot{\mathbf{J}}_{\omega_1} = [\mathbf{0}_{3 \times 1} \quad -\dot{h}\hat{\mathbf{a}}], \quad \dot{\mathbf{J}}_{\omega_2} = [\mathbf{0}_{3 \times 1} \quad +\dot{h}\hat{\mathbf{a}}], \quad (40)$$

where $\dot{h} = c \dot{\gamma}$, and the scalar parameter c is given in Appendix Appendix A. Furthermore, the derivative of the Jacobian matrices of the third and fourth links, requires the time derivatives of unit vectors $\hat{\mathbf{c}}$ and $\hat{\mathbf{d}}$ and the scalar parameter s . The time derivative of s is computed using Maple symbolic manipulation, which yields the expression of Eq. (A.4). Thence, the derivative of the Jacobian matrices of the third and fourth links are obtained as:

$$\dot{\mathbf{J}}_{\omega_3} = \dot{\mathbf{J}}_{\omega_1} + \left[\mathbf{0}_{3 \times 1} \quad -\left(\dot{s} \cdot \hat{\mathbf{b}} + s \cdot \dot{\hat{\mathbf{b}}} \right) \right], \quad \dot{\mathbf{J}}_{\omega_4} = \dot{\mathbf{J}}_{\omega_2} + \left[\mathbf{0}_{3 \times 1} \quad -\left(\dot{s} \cdot \hat{\mathbf{c}} + s \cdot \dot{\hat{\mathbf{c}}} \right) \right]. \quad (41)$$

4.2. The 3-RRR Spherical Parallel Manipulator

The 3-RRR spherical parallel manipulator is a symmetrical 3-DOF mechanism composed of three identical kinematic chains. Each kinematic chain is itself composed of a proximal and a distal link, and three revolute joints. The proximal links are driven by actuators, while distal links and the moving platform are connected together with passive revolute joints. The structure of the 3-RRR manipulator is depicted in Fig. 3. The kinematic characteristics of this robot are mentioned in details in [47], and in this article, only its important issues are reviewed.

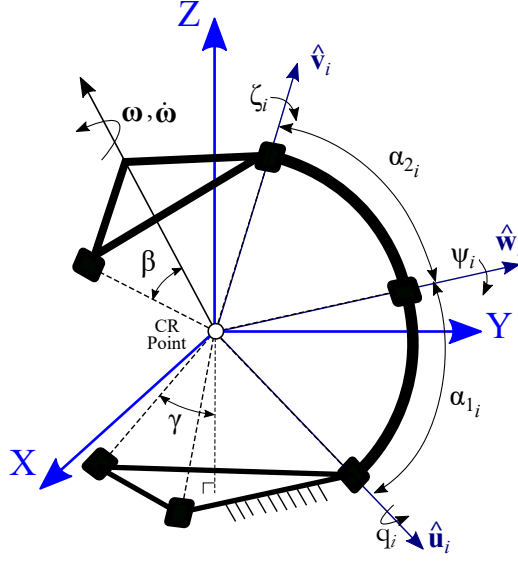


Figure 3: Schematic of a typical 3-RRR spherical parallel manipulator

4.2.1. Robot Geometry

For kinematic analysis of the 3-RRR spherical parallel manipulator, the orientation of the moving platform is described using ZYX fixed-body Euler angles. Therefore, $\theta = [\theta_1, \theta_2, \theta_3]^T$ are considered as the task space variables, Thus, the rotation matrix of the moving platform may be derived as ${}^0R_p = R_z(\theta_1)R_y(\theta_2)R_x(\theta_3)$.

In the 3-RRR manipulator, unit vectors \hat{u}_i , \hat{v}_i , and \hat{w}_i , for $i = 1, 2, 3$, all intersect at the CR point, which is defined as the origin of the base coordinate system. Therefore, the unit vector of the primary and the intermediate revolute joints can be formulated as:

$$\hat{u}_i = R_z(\lambda_i)R_x(\gamma - \pi)[0, 0, 1]^T, \quad (42a)$$

$$\hat{w}_i = R_z(\lambda_i)R_x(\gamma - \pi)R_z(q_i)R_x(\alpha_{1_i})[0, 0, 1]^T. \quad (42b)$$

Moreover, \hat{v}_i may be derived as follows:

$$\hat{v}_i^* = R_z(\eta_i)R_x(-\beta)[0, 0, 1]^T, \quad (43a)$$

$$\hat{v}_i = {}^0R_p \hat{v}_i^*, \quad (43b)$$

in which, \hat{v}_i^* represents the unit vector \hat{v}_i in the initial configuration of the moving platform.

4.2.2. Differential Kinematic Analysis

Before beginning the Jacobian analysis of the 3-RRR manipulator, it should be noted that by choosing the Euler angles as a way to describe the moving platform orientation, the angular velocity of the moving platform would not be equal to the rate of change of the Euler angles, $\dot{\theta} = [\dot{\theta}_1, \dot{\theta}_2, \dot{\theta}_3]^T$. Instead, this relationship between these two vectors would be defined as:

$${}^0\omega = E\dot{\theta}, \quad (44)$$

in which, $E(\theta_1, \theta_2, \theta_3)$ relates the rates of the Euler angles to the angular velocity of the moving platform. In the ZYX fixed body Euler angles, this matrix is given by:

$$E = \begin{bmatrix} 0 & -\sin(\theta_1) & \cos(\theta_1) \cos(\theta_2) \\ 0 & \cos(\theta_1) & \sin(\theta_1) \cos(\theta_2) \\ 1 & 0 & -\sin(\theta_2) \end{bmatrix}. \quad (45)$$

Therefore, the angular velocity of the moving platform may be derived as the sum of its successive angular rotations as:

$${}^0\boldsymbol{\omega} = \dot{q}_i \cdot \hat{\mathbf{u}}_i + \dot{\psi}_i \cdot \hat{\mathbf{w}}_i + \dot{\zeta}_i \cdot \hat{\mathbf{v}}_i. \quad (46)$$

In this equation, \dot{q}_i and $\dot{\psi}_i$ are derived by dot-multiplying both sides of the equation of (46) in $(\hat{\mathbf{v}}_i \times \hat{\mathbf{w}}_i)$ and $(\hat{\mathbf{u}}_i \times \hat{\mathbf{v}}_i)$, respectively, which results in:

$$\dot{q}_i = \frac{(\hat{\mathbf{v}}_i \times \hat{\mathbf{w}}_i)}{(\hat{\mathbf{v}}_i \times \hat{\mathbf{w}}_i) \cdot \hat{\mathbf{u}}_i} \cdot {}^0\boldsymbol{\omega} = \mathbf{J}_{\omega_i} \dot{\boldsymbol{\theta}} \quad , \quad \text{for } i = 1, 2, 3, \quad (47a)$$

$$\dot{\psi}_i = \frac{(\hat{\mathbf{u}}_i \times \hat{\mathbf{v}}_i)}{(\hat{\mathbf{u}}_i \times \hat{\mathbf{v}}_i) \cdot \hat{\mathbf{w}}_i} \cdot {}^0\boldsymbol{\omega} = \mathbf{J}_{\omega_{p_i}} \dot{\boldsymbol{\theta}} \quad , \quad \text{for } i = 1, 2, 3. \quad (47b)$$

Now, in order to derive the Jacobian matrices from equations of (47a) and (47b), the following parameters are defined for the sake of simplification:

$$\mathbf{p}_{1_i} = \hat{\mathbf{v}}_i \times \hat{\mathbf{w}}_i, \quad (48a)$$

$$\mathbf{p}_{2_i} = \hat{\mathbf{u}}_i \times \hat{\mathbf{v}}_i, \quad (48b)$$

$$h_i = (\hat{\mathbf{v}}_i \times \hat{\mathbf{w}}_i) \cdot \hat{\mathbf{u}}_i = \mathbf{p}_{1_i} \cdot \hat{\mathbf{u}}_i. \quad (48c)$$

Finally, using equations of (44), (47), and (48), each row of the input-output Jacobian and the passive Jacobian matrices are derived as:

$$\mathbf{J}_{\omega_i} = h_i^{-1} \mathbf{p}_{1_i}^T \mathbf{E}, \quad \text{for } i = 1, 2, 3, \quad (49a)$$

$$\mathbf{J}_{\omega_{p_i}} = h_i^{-1} \mathbf{p}_{2_i}^T \mathbf{E}, \quad \text{for } i = 1, 2, 3. \quad (49b)$$

4.2.3. Jacobian Analysis of Links

The angular velocity of the proximal and distal links of each kinematic chain may be written as:

$${}^0\boldsymbol{\omega}_{1_i} = \dot{q}_i \cdot \hat{\mathbf{u}}_i = \mathbf{J}_{\omega_{1_i}} \dot{\boldsymbol{\theta}}, \quad (50a)$$

$${}^0\boldsymbol{\omega}_{2_i} = {}^0\boldsymbol{\omega}_{1_i} + \dot{\psi}_i \cdot \hat{\mathbf{w}}_i = \mathbf{J}_{\omega_{2_i}} \dot{\boldsymbol{\theta}}. \quad (50b)$$

Therefore, using equations (47a) and (47b), each row of the Jacobian matrix of the proximal and distal links are formulated as follows:

$$\mathbf{J}_{\omega_{1_i}} = \hat{\mathbf{u}}_i \mathbf{J}_{\omega_i}, \quad (51a)$$

$$\mathbf{J}_{\omega_{2_i}} = \mathbf{J}_{1_i} + \hat{\mathbf{w}}_i \mathbf{J}_{\omega_{p_i}}. \quad (51b)$$

4.2.4. Acceleration Analysis

In order to derive the acceleration terms in the proposed dynamic formulation, it is necessary to obtain the time derivative of \dot{q}_i and $\dot{\psi}_i$. Thus, the time derivative of each row of the corresponding Jacobian matrices \mathbf{J}_{ω} and \mathbf{J}_{ω_p} is computed symbolically as:

$$\dot{\mathbf{j}}_{\omega_i} = \frac{\dot{\mathbf{p}}_{1_i}^T \mathbf{E} + \mathbf{p}_{1_i}^T \dot{\boldsymbol{\omega}}}{h_i} - \frac{\mathbf{p}_{1_i}^T \mathbf{E} \dot{h}_i}{h_i^2}, \quad (52)$$

$$\dot{\mathbf{j}}_{\omega_{p_i}} = \frac{\dot{\mathbf{p}}_{2_i}^T \mathbf{E} + \mathbf{p}_{2_i}^T \dot{\mathbf{E}}}{h_i} - \frac{\mathbf{p}_{2_i}^T \mathbf{E} \dot{h}_i}{h_i^2}, \quad (53)$$

In these equations, the method of calculating the time derivatives of vectors of \mathbf{p}_{1_i} and \mathbf{p}_{2_i} , and the value of scalar h_i is given in Appendix Appendix B. Therefore, the time derivative of the Jacobian matrix of the proximal and the distal links may be represented by:

$$\dot{\mathbf{J}}_{\omega_{1_i}} = \hat{\mathbf{u}}_i \dot{\mathbf{J}}_{\omega_i}, \quad (54a)$$

$$\dot{\mathbf{J}}_{\omega_{2_i}} = \dot{\mathbf{J}}_{\omega_{1_i}} + \left(\dot{\hat{\mathbf{w}}}_i \mathbf{J}_{\omega_{p_i}} + \hat{\mathbf{w}}_i \dot{\mathbf{J}}_{\omega_{p_i}} \right), \quad (54b)$$

in which, $\dot{\hat{\mathbf{w}}}_i$ is given in the Appendix Appendix B.

4.2.5. Dynamic Formulations

As mentioned earlier, the angular velocity of the moving platform is related to the Euler angles rate with ${}^0\boldsymbol{\omega} = \mathbf{E}\dot{\boldsymbol{\theta}}$. In the Jacobian analysis of each link, the effect of the \mathbf{E} matrix has been considered. Thus, the terms related to the dynamics of the moving platform given in Eq. (10a), are rewritten as follows:

$$\mathcal{J}_\omega^T \boldsymbol{\tau} = ({}^0\mathbf{I}_{\mathcal{A}_p}) {}^0\dot{\boldsymbol{\omega}} + S({}^0\boldsymbol{\omega}) ({}^0\mathbf{I}_{\mathcal{A}_p}) {}^0\boldsymbol{\omega} - m_i S({}^0\boldsymbol{\rho}_p) \mathbf{g}_0, \quad (55)$$

in which each row of the Jacobian matrix \mathcal{J}_ω is defined by $\mathcal{J}_{\omega_i} = h_i^{-1} \mathbf{p}_{1_i}^T$. Although the Eq. (55) has an explicit form, it is written based on ${}^0\boldsymbol{\omega}$ and ${}^0\dot{\boldsymbol{\omega}}$ terms, while explicit dynamics should be in terms of $\dot{\boldsymbol{\theta}}$ and $\ddot{\boldsymbol{\theta}}$ to have the same force distribution as the dynamics of each link. As a result, using the properties of ${}^0\boldsymbol{\omega} = \mathbf{E}\dot{\boldsymbol{\theta}}$ and ${}^0\dot{\boldsymbol{\omega}} = \mathbf{E}\ddot{\boldsymbol{\theta}} + \dot{\mathbf{E}}\dot{\boldsymbol{\theta}}$, and multiplying \mathbf{E}^T to the left side of the Eq. (55), the explicit dynamic of the moving platform based on $\dot{\boldsymbol{\theta}}$ and $\ddot{\boldsymbol{\theta}}$, may be written as follows:

$$\mathbf{J}_\omega^T \boldsymbol{\tau} = \mathbf{M}_p(\boldsymbol{\theta})\ddot{\boldsymbol{\theta}} + \mathbf{C}_p(\boldsymbol{\theta}, \dot{\boldsymbol{\theta}})\dot{\boldsymbol{\theta}} + \mathbf{g}_p(\boldsymbol{\theta}). \quad (56)$$

In this representation, each row of the Jacobian matrix $\mathbf{J}_{\omega_i} = \mathcal{J}_{\omega_i} \mathbf{E}$, for $i = 1, 2, 3$, is equal to each row of the Jacobian matrix of the whole manipulator, given in equation (49a). Moreover, the explicit dynamic of the moving platform may be represented by the following matrices:

$$\mathbf{M}_p = \mathbf{E}^T ({}^0\mathbf{I}_{\mathcal{A}_p}) \mathbf{E}, \quad (57a)$$

$$\mathbf{C}_p = \mathbf{E}^T ({}^0\mathbf{I}_{\mathcal{A}_p}) \dot{\mathbf{E}} + \mathbf{E}^T \left(S(\mathbf{E}\dot{\boldsymbol{\theta}}) ({}^0\mathbf{I}_{\mathcal{A}_p}) \right) \mathbf{E}, \quad (57b)$$

$$\mathbf{g}_p = -\mathbf{E}^T (m_i S({}^0\boldsymbol{\rho}_p) \mathbf{g}_0). \quad (57c)$$

The same process must be followed for the derivation of the corresponding terms related to the moving platform in the regressors. Therefore, it is enough to use ${}^0\boldsymbol{\omega}_r = \mathbf{E}\dot{\boldsymbol{\theta}}_r$ and ${}^0\dot{\boldsymbol{\omega}}_r = \mathbf{E}\ddot{\boldsymbol{\theta}}_r + \dot{\mathbf{E}}\dot{\boldsymbol{\theta}}_r$ and multiply the left side of equation (27b) by \mathbf{E}^T .

5. Verification

In order to verify the dynamic formulation proposed in this paper, two sides of the following equations are compared to each other for a typical trajectory $\boldsymbol{\theta}$:

$$\mathbf{M}(\boldsymbol{\theta})\ddot{\boldsymbol{\theta}} + \mathbf{C}(\boldsymbol{\theta}, \dot{\boldsymbol{\theta}})\dot{\boldsymbol{\theta}} + \mathbf{g}(\boldsymbol{\theta}) = \mathbf{Y}(\boldsymbol{\theta}, \dot{\boldsymbol{\theta}}, \ddot{\boldsymbol{\theta}})\boldsymbol{\pi} = \mathbf{Y}_r(\boldsymbol{\theta}, \dot{\boldsymbol{\theta}}, \ddot{\boldsymbol{\theta}})\boldsymbol{\pi}_r, \quad (58a)$$

$$\mathbf{M}(\boldsymbol{\theta})\ddot{\boldsymbol{\theta}}_r + \mathbf{C}(\boldsymbol{\theta}, \dot{\boldsymbol{\theta}}_r)\dot{\boldsymbol{\theta}}_r + \mathbf{g}(\boldsymbol{\theta}) = \mathbf{Y}_S(\boldsymbol{\theta}, \dot{\boldsymbol{\theta}}, \dot{\boldsymbol{\theta}}_r, \ddot{\boldsymbol{\theta}}_r)\boldsymbol{\pi} = \mathbf{Y}_{S_r}(\boldsymbol{\theta}, \dot{\boldsymbol{\theta}}, \dot{\boldsymbol{\theta}}_r, \ddot{\boldsymbol{\theta}}_r)\boldsymbol{\pi}_r. \quad (58b)$$

For the verification process, each robot's explicit dynamics is both coded in MATLAB and modeled in the MSC-ADAMS[®] package. In the latter case, a CAD model of the corresponding robot is used, as shown in Fig. 4a and Fig. 4b. By applying the desired trajectory $\boldsymbol{\theta} = \boldsymbol{\theta}_d$ to both models separately and comparing the resulting output torques of the actuators, one may conclude that the dynamic formulation is verified if the differences are negligible.

5.1. ARAS-Diamond Robot Verification

In order to verify the resulted dynamic formulation of the ARAS-Diamond robot, a third-order polynomial trajectory for the end-effector is considered in the task space, all of which takes about one second. In the designed trajectory, ϕ changes from $\phi_0 = 0$ to $\phi_f = 120^\circ$, while γ varies from $\gamma_0 = 70^\circ$ to $\gamma_f = 10^\circ$. Furthermore, the considered parameters of the ARAS-Diamond model are also reported in Table C.3. By applying this trajectory to the explicit dynamic formulation of the robot in MATLAB and the robot's model in MSC-ADAMS[®], the required actuators torques are determined as shown in Fig. 5a. The difference between the torques generated by both models is shown in Fig. 5b.

As shown in Figs. 5a and 5b, the explicit dynamic formulation of the ARAS-Diamond robot is verified with an accuracy of approximately 10^{-4} *N.m*. This further confirms the accuracy of the derived kinematic

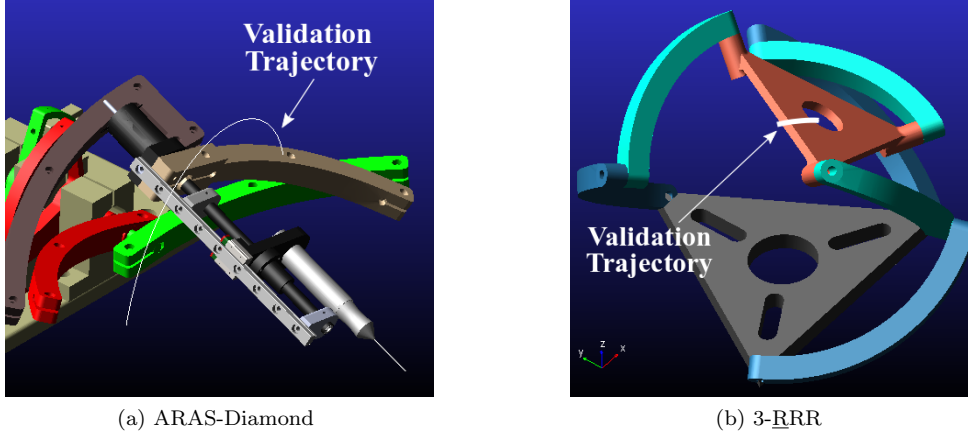


Figure 4: Considered Models in MSC-ADAMS[®]

and dynamic formulations. However, it should be noted that the main reason caused behind the validation error is the inaccuracy in measurement and parameter settings in the MSC-ADAMS[®] package. For a more definitive verification, other trajectories were tested, such as a sinusoidal and a multi-sine trajectory. In all these cases, as expected, the resulting error remain in the order of $10^{-4} N.m$.

Additionally, in order to verify the linear regressor form of the dynamic formulation and the corresponding reduced regressor form, a random trajectory $(\theta, \dot{\theta}, \ddot{\theta})$ is generated in the feasible workspace. Similarly, for the validation of the Slotine-Li regressor and its corresponding reduced regressor, a random trajectory for $(\theta, \dot{\theta}, \ddot{\theta}_r, \ddot{\theta}_r)$ is considered in the feasible workspace of the robot. In this study, the numerical difference between the left-hand sides of the equations of (58a) and (58b), representing the explicit dynamics of the robot, and their right-hand sides, are calculated and reported in Figs. 6a and 6b, respectively.

As it can be seen in these figures, the linear form of the dynamics, the Slotine-Li regressor, as well as their corresponding reduced forms differ from the explicit dynamics of the ARAS-Diamond robot with an order of $10^{-13} N.m$. This provides another validation of the proposed formulations.

5.2. 3-RRR Spherical Parallel Manipulator Verification

The same method described in section 5.1 is adopted here in order to verify the proposed dynamic formulation of the 3-RRR spherical parallel manipulator. For this purpose, a third-order polynomial trajectory

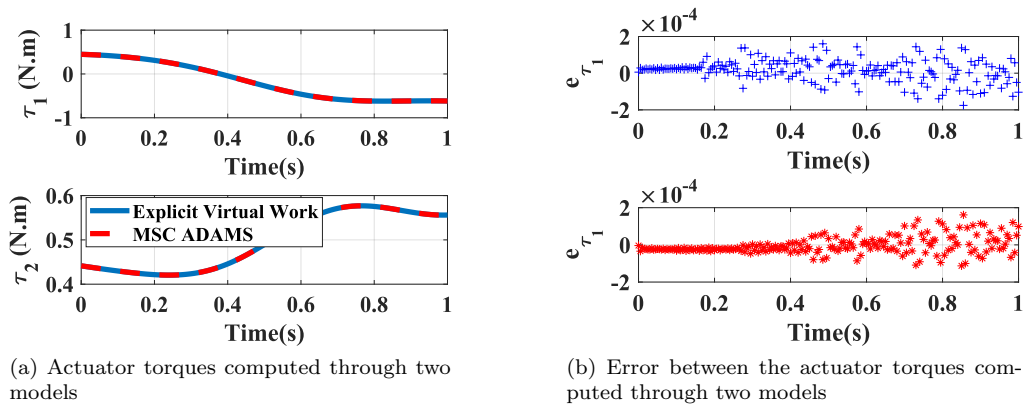


Figure 5: ARAS-Diamond explicit dynamics verification

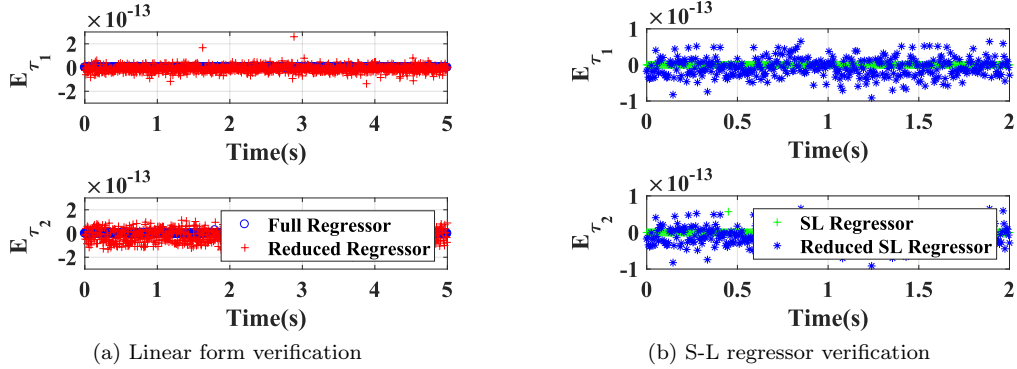


Figure 6: ARAS-Diamond linear regressors verification

is considered for the moving platform. In this trajectory, the values of θ changes from $\theta_0 = [0, 0, 0]^T$ to $\theta_f = [10^\circ, 30^\circ, 20^\circ]^T$ in one second. Besides, the parameters of the considered 3-RRR spherical parallel manipulator model have also been reported in Table C.4. The results of the dynamic verification and the validation errors are shown in Figs. 7a and 7b, respectively.

In addition, the reduced regressors and the linear and Slotine-Li regressors were compared with the explicit dynamics of the manipulator over a random trajectory within the robot feasible workspace. To prevent the article from becoming bulky, the error plots are not re-reported. The results show 10^{-14} $N.m$ accuracy between the results, and are available to everyone at the Github page.

6. Conclusions

In this paper, different forms of dynamic formulations of spherical parallel robots (SPRs) including explicit dynamics, linear and Slotine-Li (S-L) regressors were formulated to be used in the design of model-based controllers and dynamic identification schemes. To this end, the implicit dynamic of SPRs was first formulated using the principle of virtual work in task-space, and then by an extension, their explicit dynamic formulation was derived. The linear and S-L regressor forms of SPRs were then obtained using explicit dynamic, and by using the Gauss-Jordan procedure, regressor forms are reduced to a unique and

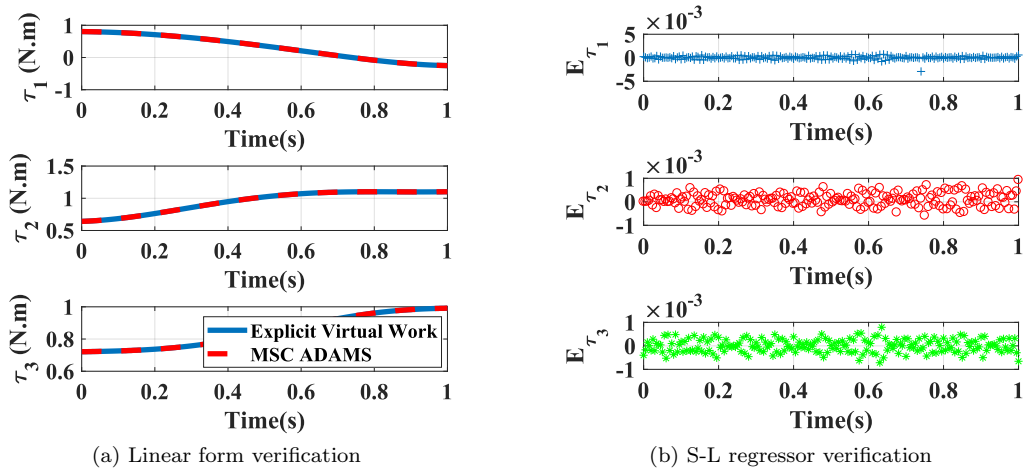


Figure 7: 3-RRR manipulator explicit dynamics verification

closed-form structure. Finally, to verify the proposed formulations, two SPR case studies, namely, the ARAS-Diamond robot and the 3-RRR spherical manipulator examined. The results of the explicit dynamics, linear regression form of robots' dynamics, S-L regressor, and the corresponding reduced form regressors were verified by comparing them with those obtained by MSC-ADAMS[®] package. The proposed method opens the possibility of implementing a wide range of adaptive model-based controllers and regressor-based identification schemes on SPRs.

Declaration of Competing Interest

The authors declare that they have no conflict of interest.

Acknowledgments

The authors appreciate the support from Iranian National Science Foundation (INSF) under grant number 99028112. Moreover, the authors greatly appreciate Mr. Sina Allahkaram, Mr. Rohollah Khorambakht, and Mr. Omid Mehdizade for their excellent feedbacks during this research.

Appendix A. Kinematic Parameters of the ARAS-Diamond

The h scalar parameter in equation (33) is defined as follows:

$$h = \frac{\cot \alpha - \cos \hat{A} \cdot \cot \gamma}{\sin \hat{A}}. \quad (\text{A.1})$$

It was stated that equation of $\dot{\hat{B}} = -\dot{\hat{C}} = s \dot{\gamma}$ may be derived in such a way that s is expressed as:

$$s = \frac{\cos \gamma \cdot \sin \hat{A} + h \sin \gamma \cdot \cos \hat{A}}{\cos \hat{B} \cdot \sin \beta}. \quad (\text{A.2})$$

Furthermore, c scalar parameter in the equation of $\dot{h} = c \dot{\gamma}$ may be derived as:

$$c = \frac{h \cdot \sin \gamma \left(\cos \alpha \cdot \cos \hat{A} - \sin \alpha \cdot \cos \gamma \right) - \sin \hat{A} \cdot \cos \hat{A} \cdot \sin \alpha}{\sin^2 \gamma \cdot \sin \alpha \cdot \sin^2 \hat{A}}. \quad (\text{A.3})$$

In order to evaluate the derivative of the Jacobian matrix of the third and the fourth links in equation of (41), it is necessary to compute the derivative of s , which yields to:

$$\dot{s} = \frac{\dot{s}_n}{\dot{s}_d}, \quad (\text{A.4})$$

in which,

$$\begin{aligned} \dot{s}_n = & + h \dot{\gamma} \cdot \cos \hat{B} \left(-h \sin \hat{A} \cdot \sin \gamma + \cos \hat{A} \cdot \cos \gamma \right) + s \dot{\gamma} \cdot \sin \hat{B} \left(+h \cos \hat{A} \cdot \sin \gamma + \sin \hat{A} \cdot \cos \gamma \right) \\ & + \cos \hat{B} \left(\dot{\gamma} \left(+h \cos \gamma \cdot \cos \hat{A} - \sin \hat{A} \cdot \sin \gamma \right) + c \dot{\gamma} \cdot \sin \gamma \cdot \cos \hat{A} \right), \end{aligned} \quad (\text{A.5})$$

$$\dot{s}_d = \cos^2 \hat{B} \cdot \sin \beta. \quad (\text{A.6})$$

Appendix B. Kinematic Parameters of the 3-RRR Manipulator

As mentioned before, the acceleration formulations of the 3-RRR manipulator are based on the derivative of the vectors of \mathbf{p}_{1_i} , \mathbf{p}_{2_i} , and the scalar parameter of h_i . Using equations of (42) and (43), the following formulas are easily extractable:

$$\dot{\hat{\mathbf{u}}}_i = 0, \quad (\text{B.1a})$$

$$\dot{\hat{\mathbf{v}}}_i = {}^0\dot{\mathbf{R}}_p \hat{\mathbf{v}}_i^*, \quad (\text{B.1b})$$

$$\dot{\hat{\mathbf{w}}}_i = \mathbf{R}_z(\lambda_i)\mathbf{R}_x(\gamma - \pi)\dot{\mathbf{R}}_z(q_i)\mathbf{R}_x(\alpha_{1_i})[0, 0, 1]^T, \quad (\text{B.1c})$$

in which, $\dot{\mathbf{R}}_z$ and ${}^0\dot{\mathbf{R}}_p$ denote the time derivative of the rotation matrices of \mathbf{R}_z and ${}^0\mathbf{R}_p$, respectively. Therefore, according to Eq. (48), the following derivatives may easily be determined:

$$\dot{\mathbf{p}}_{1_i} = \dot{\hat{\mathbf{v}}}_i \times \hat{\mathbf{w}} + \hat{\mathbf{v}} \times \dot{\hat{\mathbf{w}}}_i, \quad (\text{B.2a})$$

$$\dot{\mathbf{p}}_{2_i} = \hat{\mathbf{u}} \times \dot{\hat{\mathbf{v}}}_i, \quad (\text{B.2b})$$

$$\dot{h}_i = \dot{\mathbf{p}}_{1_i} \cdot \hat{\mathbf{u}}. \quad (\text{B.2c})$$

Appendix C. Parameters for Verification

Table C.3: Considered parameters of ARAS-Diamond

Symbol	Description	Value
$\alpha = \beta$	Angular length of links	45° deg
m	Mass of links	$[0.117, 0.112, 0.155, 0.145]^T$ kg
${}^1\rho_1$	CM of link1	$[0.098, 0, 0.232]^T$ m
${}^2\rho_2$	CM of link2	$[0.087, 0, 0.210]^T$ m
${}^3\rho_3$	CM of link3	$[0.107, 0, 0.254]^T$ m
${}^4\rho_4$	CM of link4	$[0.078, 0, 0.188]^T$ m
${}^1\mathbf{I}_1$	MI of link1	$diag(6.440, 6.350, 1.716)10^{-4}$ kg.m ²
${}^2\mathbf{I}_2$	MI of link2	$diag(5.359, 5.284, 0.150)10^{-4}$ kg.m ²
${}^3\mathbf{I}_3$	MI of link3	$diag(9.849, 9.342, 0.610)10^{-4}$ kg.m ²
${}^4\mathbf{I}_4$	MI of link4	$diag(7.577, 7.496, 2.348)10^{-4}$ kg.m ²

References

References

- [1] S. Bai, X. Li, and J. Angeles, "A review of spherical motion generation using either spherical parallel manipulators or spherical motors," *Mechanism and Machine Theory*, vol. 140, pp. 377 – 388, 2019.
- [2] H. Li, J. Luo, C. Huang, Q. Huang, and S. Xie, "Design and control of 3-dof spherical parallel mechanism robot eyes inspired by the binocular vestibule-ocular reflex," *Journal of Intelligent & Robotic Systems*, vol. 78, no. 3-4, pp. 425–441, 2015.
- [3] A. Bataleblu, M. Motaharifar, E. Abedlu, and H. D. Taghirad, "Robust h_∞ control of a 2rt parallel robot for eye surgery," in *2016 4th International Conference on Robotics and Mechatronics (ICROM)*. IEEE, 2016, pp. 136–141.
- [4] J. Angeles and S. K. Lee, "The formulation of dynamical equations of holonomic mechanical systems using a natural orthogonal complement," *Journal of Applied Mechanics*, vol. 55, no. 1, pp. 243–244, mar 1988.
- [5] W. Khalil and F. Bennis, "Symbolic calculation of the base inertial parameters of closed-loop robots," *The International Journal of Robotics Research*, vol. 14, no. 2, pp. 112–128, apr 1995.
- [6] A. Codourey, "Dynamic modeling of parallel robots for computed-torque control implementation," *The International Journal of Robotics Research*, vol. 17, no. 12, pp. 1325–1336, dec 1998.
- [7] B. Dasgupta and T. Mruthyunjaya, "Closed-form dynamic equations of the general stewart platform through the newton–euler approach," *Mechanism and Machine Theory*, vol. 33, no. 7, pp. 993–1012, oct 1998.

Table C.4: Considered parameters of the considered 3-RRR SPR

Symbol	Description	Value
$\boldsymbol{\eta} = \boldsymbol{\lambda}$	Structural angles	$[0, 120^\circ, 240^\circ]^T$ deg
β	Base regular pyramid	$\arccos(\frac{\sqrt{3}}{3})$ deg
γ	Moving platform regular pyramid	$\arcsin(\frac{\sqrt{3}}{3})$ deg
α_{1_i}	Proximal links length	80° deg
α_{2_i}	Distal links length	$\alpha_{2_i} = 70^\circ$ deg
m_p	Mass of moving platform	0.604 kg
$m_{1_1} = m_{1_2} = m_{1_3}$	Mass of proximal links	0.501 kg
$m_{2_1} = m_{2_2} = m_{2_3}$	Mass of distal links	0.389 kg
${}^p \boldsymbol{\rho}_p$	CM of moving platform	$[0, 0, 0.084]^T$ m
${}^1 \boldsymbol{\rho}_{1_1} = {}^1 \boldsymbol{\rho}_{1_2} = {}^1 \boldsymbol{\rho}_{1_3}$	CM of proximal links	$[0, -0.117, 0.139]^T$ m
${}^2 \boldsymbol{\rho}_{2_1} = {}^2 \boldsymbol{\rho}_{2_2} = {}^2 \boldsymbol{\rho}_{2_3}$	CM of distal links	$[0, -0.093, 0.133]^T$ m
${}^p \mathbf{I}_p$	MI of moving platform	$\text{diag}(0.003, 0.001, 0.001)$ kg.m ²
${}^1 \mathbf{I}_{1_1} = {}^1 \mathbf{I}_{1_2} = {}^1 \mathbf{I}_{1_3}$	MI of proximal links	$\text{diag}(0.003, 0.003, 0)$ kg.m ²
${}^2 \mathbf{I}_{2_1} = {}^2 \mathbf{I}_{2_2} = {}^2 \mathbf{I}_{2_3}$	MI of distal links	$\text{diag}(0.001, 0.001, 0)$ kg.m ²

- [8] J. Wang and C. M. Gosselin, "A new approach for the dynamic analysis of parallel manipulators," *Multibody System Dynamics*, vol. 2, no. 3, pp. 317–334, 1998.
- [9] L.-W. Tsai, "Solving the inverse dynamics of a stewart-gough manipulator by the principle of virtual work," *Journal of Mechanical Design*, vol. 122, no. 1, pp. 3–9, dec 1999.
- [10] W. Khalil and S. Guegan, "Inverse and direct dynamic modeling of gough–stewart robots," *IEEE Transactions on Robotics*, vol. 20, no. 4, pp. 754–762, aug 2004.
- [11] W. Khalil and O. Ibrahim, "General solution for the dynamic modeling of parallel robots," *Journal of Intelligent and Robotic Systems*, vol. 49, no. 1, pp. 19–37, mar 2007.
- [12] H. Abdellatif and B. Heimann, "Computational efficient inverse dynamics of 6-DOF fully parallel manipulators by using the lagrangian formalism," *Mechanism and Machine Theory*, vol. 44, no. 1, pp. 192–207, jan 2009.
- [13] M. Díaz-Rodríguez, V. Mata, Á. Valera, and Á. Page, "A methodology for dynamic parameters identification of 3-DOF parallel robots in terms of relevant parameters," *Mechanism and Machine Theory*, vol. 45, no. 9, pp. 1337–1356, sep 2010.
- [14] R. Oftadeh, M. M. Aref, and H. D. Taghirad, "Explicit dynamics formulation of stewart-gough platform: A newton-euler approach," in *2010 IEEE/RSJ International Conference on Intelligent Robots and Systems*. IEEE, oct 2010.
- [15] F. C. Park, B. Kim, C. Jang, and J. Hong, "Geometric algorithms for robot dynamics: A tutorial review," *Applied Mechanics Reviews*, vol. 70, no. 1, jan 2018.
- [16] A. Müller, "Dynamics modeling of topologically simple parallel kinematic manipulators: A geometric approach," *Applied Mechanics Reviews*, vol. 72, no. 3, dec 2019.
- [17] L.-W. Tsai, *Robot analysis: the mechanics of serial and parallel manipulators*. John Wiley & Sons, 1999.
- [18] J. Angeles, *Fundamentals of Robotic Mechanical Systems*. Springer US, 2007.
- [19] S. V. Shah, S. K. Saha, and J. K. Dutt, "Dynamics of tree-type robotic systems," in *Dynamics of tree-type robotic systems*. Springer, 2013, pp. 73–88.
- [20] H. D. Taghirad, *Parallel Robots*. CRC Press, feb 2013.
- [21] S. Briot, W. Khalil *et al.*, "Dynamics of parallel robots," *From rigid bodies to flexible elements*. Springer, 2015.
- [22] S. Staicu, *Dynamics of Parallel Robots*. Springer International Publishing, 2019.
- [23] F. Paccot, N. Andreff, and P. Martinet, "A review on the dynamic control of parallel kinematic machines: Theory and experiments," *The International Journal of Robotics Research*, vol. 28, no. 3, pp. 395–416, mar 2009.
- [24] J. J. Craig, P. Hsu, and S. S. Sastry, "Adaptive control of mechanical manipulators," *The International Journal of Robotics Research*, vol. 6, no. 2, pp. 16–28, 1987.
- [25] M. W. Spong and R. Ortega, "On adaptive inverse dynamics control of rigid robots," *IEEE Transactions on Automatic Control*, vol. 35, no. 1, pp. 92–95, 1990.
- [26] M. Grotjahn, B. Heimann, and H. Abdellatif, "Identification of friction and rigid-body dynamics of parallel kinematic structures for model-based control," *Multibody System Dynamics*, vol. 11, no. 3, pp. 273–294, 2004.
- [27] J. Wu, J. Wang, and Z. You, "An overview of dynamic parameter identification of robots," *Robotics and Computer-Integrated Manufacturing*, vol. 26, no. 5, pp. 414 – 419, 2010.
- [28] J.-J. E. Slotine and W. Li, "On the adaptive control of robot manipulators," *The International Journal of Robotics Research*, vol. 6, no. 3, pp. 49–59, 1987.
- [29] M. Malosio, S. P. Negri, N. Pedrocchi, F. Vicentini, M. Caimmi, and L. M. Tosatti, "A spherical parallel three degrees-of-freedom robot for ankle-foot neuro-rehabilitation," in *2012 Annual international conference of the IEEE engineering in medicine and biology society*. IEEE, 2012, pp. 3356–3359.
- [30] M. E. Hesar, M. Masouleh, A. Kalhor, M. Menhaj, and N. Kashi, "Ball tracking with a 2-DOF spherical parallel robot

- based on visual servoing controllers,” in *2014 Second RSI/ISM International Conference on Robotics and Mechatronics (ICRoM)*. IEEE, oct 2014.
- [31] A. Safaryazdi, M. Zarei, O. Abolghasemi, and M. T. Masouleh, “Experimental study on the model-based control of a 2-degree-of-freedom spherical parallel robot camera stabilizer based on multi-thread programming concept,” *Proceedings of the Institution of Mechanical Engineers, Part C: Journal of Mechanical Engineering Science*, vol. 232, no. 10, pp. 1882–1897, may 2017.
- [32] B. Danaei, M. Alipour, A. Arian, M. T. Masouleh, and A. Kalhor, “Control of a two degree-of-freedom parallel robot as a stabilization platform,” in *2017 5th RSI International Conference on Robotics and Mechatronics (ICRoM)*. IEEE, oct 2017.
- [33] S. A. Rad, M. G. Tamizi, M. Azmoun, M. T. Masouleh, and A. Kalhor, “Experimental study on robust adaptive control with insufficient excitation of a 3-DOF spherical parallel robot for stabilization purposes,” *Mechanism and Machine Theory*, vol. 153, p. 104026, nov 2020.
- [34] A. Bataleblu, R. Khorrambakht, and H. D. Taghirad, “Robust H_{∞} -based control of ARAS-diamond: A vitrectomy eye surgery robot,” *Proceedings of the Institution of Mechanical Engineers, Part C: Journal of Mechanical Engineering Science*, p. 095440622097933, dec 2020.
- [35] H. Saafi, M. A. Laribi, and S. Zeghloul, “Redundantly actuated 3-RRR spherical parallel manipulator used as a haptic device: improving dexterity and eliminating singularity,” *Robotica*, vol. 33, no. 5, pp. 1113–1130, jul 2014.
- [36] L. Birglen, C. Gosselin, N. Pouliot, B. Monsarrat, and T. Laliberte, “SHaDe, a new 3-DOF haptic device,” *IEEE Transactions on Robotics and Automation*, vol. 18, no. 2, pp. 166–175, apr 2002.
- [37] L. Liu, X. Song, J. Liu, W. Chen, and G. Yang, “Dynamic modeling and control methods of a novel electromagnetic-driven spherical motion generator,” in *2020 15th IEEE Conference on Industrial Electronics and Applications (ICIEA)*. IEEE, nov 2020.
- [38] X. Li, J. Liu, W. Chen, and S. Bai, “Integrated design, modeling and analysis of a novel spherical motion generator driven by electromagnetic principle,” *Robotics and Autonomous Systems*, vol. 106, pp. 69–81, aug 2018.
- [39] X. Li, S. Bai, and O. Madsen, “Dynamic modeling and trajectory tracking control of an electromagnetic direct driven spherical motion generator,” *Robotics and Computer-Integrated Manufacturing*, vol. 59, pp. 201–212, oct 2019.
- [40] A. Arian, B. Danaei, and M. T. Masouleh, “Kinematics and dynamics analysis of a 2-DOF spherical parallel robot,” in *2016 4th International Conference on Robotics and Mechatronics (ICROM)*. IEEE, oct 2016.
- [41] G. Wu, S. Caro, S. Bai, and J. Kepler, “Dynamic modeling and design optimization of a 3-DOF spherical parallel manipulator,” *Robotics and Autonomous Systems*, vol. 62, no. 10, pp. 1377–1386, oct 2014.
- [42] J. Gallardo, J. Rico, A. Frisoli, D. Checcacci, and M. Bergamasco, “Dynamics of parallel manipulators by means of screw theory,” *Mechanism and Machine Theory*, vol. 38, no. 11, pp. 1113–1131, nov 2003.
- [43] M. Ruggiu, “Kinematic and dynamic analysis of a two-degree-of-freedom spherical wrist,” *Journal of Mechanisms and Robotics*, vol. 2, no. 3, jul 2010.
- [44] J. Enferadi and A. A. Tootoonchi, “Inverse dynamics analysis of a general spherical star-triangle parallel manipulator using principle of virtual work,” *Nonlinear Dynamics*, vol. 61, no. 3, pp. 419–434, mar 2010.
- [45] J. Enferadi and V. Saffar, “A virtual power algorithm for dynamics analysis of a 3-RRcP spherical parallel robot using the screw theory,” *Australian Journal of Mechanical Engineering*, vol. 18, no. 3, pp. 351–363, oct 2018.
- [46] S. Staicu, “Recursive modelling in dynamics of agile wrist spherical parallel robot,” *Robotics and Computer-Integrated Manufacturing*, vol. 25, no. 2, pp. 409–416, apr 2009.
- [47] E. Abedloo, A. Molaei, and H. D. Taghirad, “Closed-form dynamic formulation of spherical parallel manipulators by gibbs-appell method,” in *2014 Second RSI/ISM International Conference on Robotics and Mechatronics (ICRoM)*. IEEE, 2014, pp. 576–581.
- [48] A. Akbarzadeh, J. Enferadi, and M. Sharifnia, “Dynamics analysis of a 3-RRP spherical parallel manipulator using the natural orthogonal complement,” *Multibody System Dynamics*, vol. 29, no. 4, pp. 361–380, jul 2012.
- [49] R. D. Gregorio and V. Parenti-Castelli, “Dynamics of a class of parallel wrists,” *Journal of Mechanical Design*, vol. 126, no. 3, pp. 436–441, oct 2003.
- [50] A. Akbarzadeh and J. Enferadi, “A virtual work based algorithm for solving direct dynamics problem of a 3-RRP spherical parallel manipulator,” *Journal of Intelligent & Robotic Systems*, vol. 63, no. 1, pp. 25–49, nov 2010.
- [51] S. Zarkandi, “Task-based torque minimization of a 3-PRR spherical parallel manipulator,” *Robotica*, pp. 1–30, jun 2021.
- [52] B. Danaei, A. Arian, M. T. Masouleh, and A. Kalhor, “Dynamic modeling and base inertial parameters determination of a 2-DOF spherical parallel mechanism,” *Multibody System Dynamics*, vol. 41, no. 4, pp. 367–390, jun 2017.
- [53] Q. Leboutet, J. Roux, A. Janot, J. R. Guadarrama-Olvera, and G. Cheng, “Inertial parameter identification in robotics: A survey,” *Applied Sciences*, vol. 11, no. 9, p. 4303, may 2021.
- [54] M. W. Spong and M. Vidyasagar, *Robot dynamics and control*. John Wiley & Sons, 2008.
- [55] M. R. J. Harandi, S. Khalilpour, H. D. Taghirad, and J. G. Romero, “Adaptive control of parallel robots with uncertain kinematics and dynamics,” *Mechanical Systems and Signal Processing*, vol. 157, p. 107693, 2021.
- [56] A. Codourey and E. Burdet, “A body-oriented method for finding a linear form of the dynamic equation of fully parallel robots,” in *Proceedings of international conference on robotics and automation*, vol. 2. IEEE, 1997, pp. 1612–1618.
- [57] J. Klodmann, D. Lakatos, C. Ott, and A. Albu-Schäffer, “A closed-form approach to determine the base inertial parameters of complex structured robotic systems,” *IFAC-PapersOnLine*, vol. 48, no. 1, pp. 316 – 321, 2015, 8th Vienna International Conferenceon Mathematical Modelling.
- [58] L. Nie, H. Ding, A. Kecskeméthy, J. Gan, J. Wang, and K. Ion Ting, “Singularity and branch identification of a 2 degree-of-freedom (DOF) seven-bar spherical parallel manipulator,” *Mechanical Sciences*, vol. 11, no. 2, pp. 381–393, oct 2020.

- [59] J. M. Wiitala and M. M. Stanisic, "Design of an overconstrained and dextrous spherical wrist," *Journal of Mechanical Design*, vol. 122, no. 3, pp. 347–353, dec 1998.
- [60] X. Kong, "Forward displacement analysis of a 2-dof RR-RRR-RRR spherical parallel manipulator," in *Proceedings of 2010 IEEE/ASME International Conference on Mechatronic and Embedded Systems and Applications*. IEEE, jul 2010.
- [61] X. Duan, Y. Yang, and B. Cheng, "Modeling and analysis of a 2-DOF spherical parallel manipulator," *Sensors*, vol. 16, no. 9, p. 1485, sep 2016.
- [62] C. M. Gosselin and J.-F. Hamel, "The agile eye: a high-performance three-degree-of-freedom camera-orienting device," in *Proceedings of the 1994 IEEE international conference on robotics and automation*. IEEE, 1994, pp. 781–786.
- [63] Y. Du, R. Li, D. Li, and S. Bai, "An ankle rehabilitation robot based on 3-RRS spherical parallel mechanism," *Advances in Mechanical Engineering*, vol. 9, no. 8, p. 168781401771811, aug 2017.
- [64] A. Molaie, E. Abedloo, H. D. Taghirad, and Z. Marvi, "Kinematic and workspace analysis of diamond: An innovative eye surgery robot," in *2015 23rd Iranian Conference on Electrical Engineering*, 2015, pp. 882–887.